Washington University School of Medicine
Digital Commons@Becker

Open Access Publications

9-3-2019

Wnd/DLK is a critical target of FMRP responsible for neurodevelopmental and behavior defects in the Drosophila model of fragile X syndrome

Alexandra Russo
Washington University School of Medicine in St. Louis

Aaron DiAntonio
Washington University School of Medicine in St. Louis

Follow this and additional works at: https://digitalcommons.wustl.edu/open_access_pubs

Recommended Citation
Russo, Alexandra and DiAntonio, Aaron, ,"Wnd/DLK is a critical target of FMRP responsible for neurodevelopmental and behavior defects in the Drosophila model of fragile X syndrome." Cell reports.,. . (2019).
https://digitalcommons.wustl.edu/open_access_pubs/8114

This Open Access Publication is brought to you for free and open access by Digital Commons@Becker. It has been accepted for inclusion in Open Access Publications by an authorized administrator of Digital Commons@Becker. For more information, please contact engeszer@wustl.edu.

Article

Cell Reports

Wnd/DLK Is a Critical Target of FMRP Responsible for Neurodevelopmental and Behavior Defects in the *Drosophila* Model of Fragile X Syndrome

Graphical Abstract

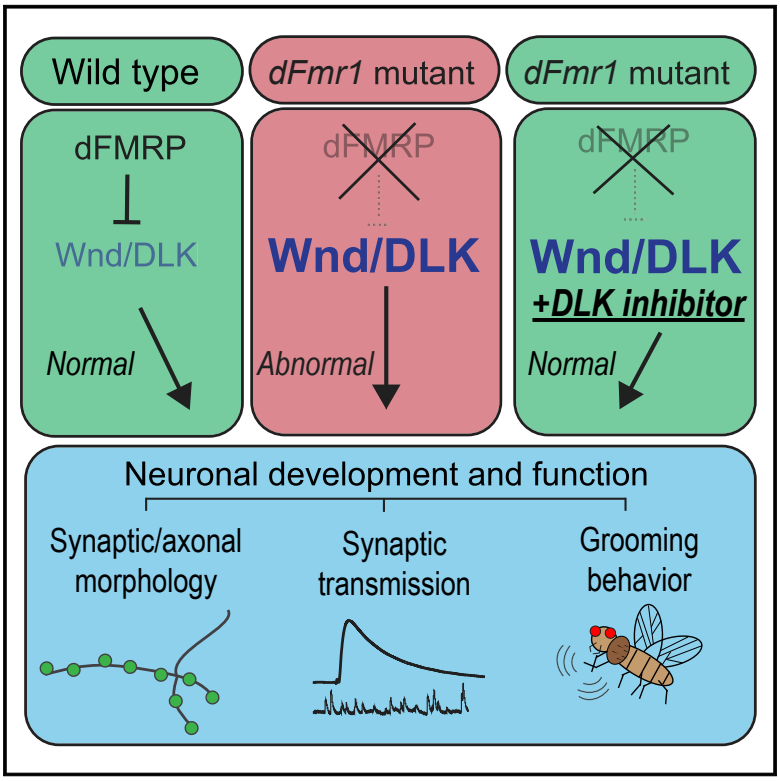

Highlights

- *Drosophila* dFMRP regulates MAP3K Wnd/DLK to promote nervous system function
- Loss of dFMRP drives increased levels of Wnd/DLK protein in the nervous system
- Increased Wnd in *dFmr1* mutants causes defects in neuronal development and behavior
- Wnd elimination or inhibition suppresses mutant phenotypes in the fly model of FXS

Authors

Alexandra Russo, Aaron DiAntonio

Correspondence

diantonio@wustl.edu

In Brief

Russo and DiAntonio identify a dysregulated MAPK signaling pathway in the fly model of fragile X syndrome. MAP3K Wnd/DLK drives *dFmr1* mutant phenotypes, and pharmacological inhibition of Wnd/DLK prevents neural dysfunction in this model, thus highlighting a possible role for Wnd/DLK in the pathophysiology of fragile X syndrome.

Russo & DiAntonio, 2019, Cell Reports *28*, 2581–2593
September 3, 2019 © 2019 The Author(s).
https://doi.org/10.1016/j.celrep.2019.08.001

CellPress

Cell Reports
Article

OPEN ACCESS
CellPress

Wnd/DLK Is a Critical Target of FMRP Responsible for Neurodevelopmental and Behavior Defects in the *Drosophila* Model of Fragile X Syndrome

Alexandra Russo[1] and Aaron DiAntonio[1,2,3,*]
[1]Department of Developmental Biology, Washington University School of Medicine in St. Louis, St. Louis, MO 63110, USA
[2]Needleman Center for Neurometabolism and Axonal Therapeutics, Washington University School of Medicine in St. Louis, St. Louis, MO 63110, USA
[3]Lead Contact
*Correspondence: diantonio@wustl.edu
https://doi.org/10.1016/j.celrep.2019.08.001

SUMMARY

Fragile X syndrome (FXS) is the leading heritable cause of intellectual disability and commonly co-occurs with autism spectrum disorder. Silencing of the Fmr1 gene leads to the absence of the protein product, fragile X mental retardation protein (FMRP), which represses translation of many target mRNAs. Excess translation of these targets is one cause of neuronal dysfunction in FXS. Utilizing the *Drosophila* model of FXS, we identified the mitogen-activated protein kinase kinase kinase (MAP3K) Wallenda/dual leucine zipper kinase (DLK) as a critical target of FMRP. dFMRP binds Wallenda mRNA and is required to limit Wallenda protein levels. In dFmr1 mutants, Wallenda signaling drives defects in synaptic development, neuronal morphology, and behavior. Pharmacological inhibition of Wallenda in larvae suppresses dFmr1 neurodevelopmental phenotypes, while adult administration prevents dFmr1 behavioral defects. We propose that in dFmr1 mutants chronic Wallenda/DLK signaling disrupts nervous system development and function and that inhibition of this kinase cascade might be a candidate therapeutic intervention for the treatment of FXS.

INTRODUCTION

Fragile X syndrome (FXS) is the most commonly inherited form of intellectual disability and is a leading cause of autism spectrum disorders (Bassell and Warren, 2008; Crawford et al., 2001). FXS is caused by a defect in the gene *Fmr1*, resulting in the absence of the *Fmr1* gene product fragile X mental retardation protein (FMRP) (Pieretti et al., 1991; Warren and Nelson, 1994). The loss of FMRP drives a host of neurological symptoms of varying severity, including learning disabilities, behavioral deficits, sensory integration issues, and an increased propensity toward seizures (Bailey et al., 2000; Berry-Kravis et al., 2010; Contractor et al., 2015). One role of FMRP is to act as an RNA-binding protein (RNA-BP) that targets mRNAs and represses translation by stalling the ribosome and preventing the transcript from being translated into protein (Bassell and Warren, 2008). FMRP is a highly conserved protein, with orthologs in mice (FMRP) and *Drosophila* (dFMRP). The absence of FMRP in animal models causes abnormal neuronal morphology, physiology, and defects in behaviors such as hyperactivity, social assays, and sleep (Bardoni and Mandel, 2002; Bhogal and Jongens, 2010). Many mRNA targets of FMRP have been identified and are highly enriched for transcripts encoding proteins that govern synaptic development and function (Ascano et al., 2012; Darnell et al., 2011). For many target transcripts, the protein products are present at elevated levels in Fmr1-knockout neurons due to the loss of translational repression. Unfortunately, efforts to treat FXS by inhibiting or downregulating these target proteins have not succeeded (Erickson et al., 2017; Lee et al., 2018).

Defining the molecular factors underlying the neurobiological defects in FXS is critical to identify candidate therapies. The *Drosophila* model of FXS, in which the single ortholog of *Fmr1*, *dFmr1*, has been mutated and causes the absence of dFMRP, has been extremely fruitful in this context (Wan et al., 2000b). dFMRP is the lone ortholog of three human Fmr1 protein products—FMR1, FXR1, and FXR2—yet only expression of human FMR1 is sufficient to rescue neurological dysfunction in the *Drosophila* model of FXS (Coffee et al., 2010), highlighting the functional conservation between dFMRP and FMR1. *dFmr1* mutants exhibit abnormal synaptic morphology and physiology at the larval neuromuscular junction (NMJ), which parallel observations of cortical and hippocampal neurons in the $Fmr1^{KO}$ mouse (Zhang et al., 2001; Comery et al., 1997; The Dutch-Belgian Fragile X Consortium, 1994). Adult flies also exhibit abnormal brain morphology and deficits in behaviors such as repetitive motions, learning and memory, and sleep (Dockendorff et al., 2002; Michel et al., 2004; Tauber et al., 2011). Hence, *Drosophila* is a powerful model to identify the molecular drivers of nervous system defects in FXS.

Studies of the larval NMJ have defined molecular pathways regulating neuronal development and function. We previously identified the conserved mitogen-activated protein kinase kinase kinase (MAP3K) Wallenda (Wnd) as a potent promoter of synaptic growth at the larval NMJ (Collins et al., 2006). Wnd and its mammalian ortholog dual leucine zipper kinase (DLK) have since been characterized as master regulators of neuronal stress pathways (Asghari Adib et al., 2018; Gerdts et al., 2016; Simon and Watkins, 2018). Activation of Wnd/DLK signaling

This is an open access article under the CC BY-NC-ND license (http://creativecommons.org/licenses/by-nc-nd/4.0/).

triggers activation of downstream kinases and transcription factors that promote a stress response. Chronic activation of this stress response induces neuronal dysfunction in neurodegenerative disorders (Pichon et al., 2017). There is substantial evidence that the molecular pathways involved in the progression of neurodegenerative diseases are similarly dysregulated in neurodevelopmental disorders, including FXS, autism, and Down syndrome (Wang, 2015). Could dysregulated Wnd/DLK signaling, and subsequent upregulation of a conserved stress pathway, have a role in the pathophysiology of neurodevelopmental disorders? In seeking regulatory mechanisms controlling Wnd/DLK activity during synaptic development, we discovered that dFMRP regulates Wnd levels and function.

FMRP targets an estimated 4% of all neuronal mRNAs for translational repression (Ashley et al., 1993; Brown et al., 2001), so multiple targets likely account for the widespread and varied defects observed when FMRP-mediated translational control is lost. Nonetheless, there may be critical targets that are responsible for multiple phenotypes. Here, we identify the MAP3K Wnd/DLK as such a key target of dFMRP. dFMRP binds *wnd* mRNA and limits Wnd protein levels. Moreover, Wnd is required for defects in neuronal morphology, physiology, and behavior in the fly FXS model. Pharmacological inhibition of Wnd in *dFmr1* mutant larvae corrects neurodevelopmental defects, while Wnd inhibition in the adult is sufficient to prevent behavioral defects in *dFmr1* mutant flies. Taken together, these findings show that dysregulated Wnd signaling is a central driver of neural dysfunction in the fly model of FXS. We propose that the Wnd/DLK stress pathway may be an exciting candidate therapeutic target for FXS.

RESULTS

Overexpressing dFMRP Suppresses *hiw* Mutant Synaptic Overgrowth by Decreasing Levels of the Conserved MAP3K Wnd

We conducted an *in vivo* genetic screen in *Drosophila* to identify regulators of the conserved MAP3K Wnd. We leveraged *Drosophila* larvae mutant for the E3 ubiquitin ligase *highwire* (*hiw*). *hiw* mutant larvae exhibit dramatic overgrowth at the larval neuromuscular junction, defined by an increased branching of the synaptic terminal nerve and a substantial increase in the number of presynaptic boutons (Figure 1A; Collins et al., 2006). We previously identified Wnd as the Hiw target responsible for driving this extensive overgrowth, demonstrating that (1) Wnd protein levels are significantly increased in the *hiw* mutant nervous system, (2) the overgrowth phenotype is entirely suppressed in *hiw;wnd* double mutants, and (3) *hiw*-dependent NMJ overgrowth is a downstream readout of MAP kinase (MAPK) signaling through JNK and Fos (Collins et al., 2006). Thus, we reasoned that overexpressing proteins that normally limit Wnd protein levels or Wnd signaling would also suppress the *hiw* mutant overgrowth phenotype at the larval NMJ. We conducted a screen in *hiw* mutants to identify candidate genes with regulatory control over Wnd. We screened through transgenic constructs enriched for (1) genes with roles in nervous system development and (2) genes with orthologs for disease-related genes in mammals, and we examined NMJ morphology in these larvae to determine if overexpression suppressed *hiw* mutant overgrowth.

The strongest hit from this screen was overexpression of *Drosophila* FMRP (dFMRP), which is encoded by the *dFmr1* gene. *hiw* mutants exhibit increased branching and bouton number at the larval NMJ compared to wild type (WT), and driving a Wnd-RNAi in the nervous system of *hiw* mutants fully suppresses the overgrowth phenotype (Figures 1A and 1B). Overexpressing dFMRP in the *hiw* mutant phenocopied Wnd knockdown by completely suppressing NMJ overgrowth (Figures 1A and 1B), restoring the number of synaptic boutons to wild-type levels (Figure 1B). Overexpression of dFMRP suppresses synaptic overgrowth in a second *hiw* mutant allele (Figures S1A and S1B), demonstrating that suppression is not an allele-specific effect. Overexpression of dFMRP in an otherwise wild-type background does not significantly alter the bouton number at the NMJ (Figures S1A and S1B), consistent with dFMRP blocking *hiw*-dependent signaling rather than inhibiting a parallel synaptic growth pathway. These results are consistent with a prior study that demonstrated overexpression of dFMRP can suppress morphological defects in *hiw* mutant class IV dendritic arborization (C4da) sensory neurons (Kim et al. 2013). Kim et al. demonstrated that FMRP represses translation of Dscam1 and that Wnd signaling enhances Dscam1 translation, and so they proposed a model in which FMRP and Wnd act antagonistically to tune Dscam1 levels. However, we found that while expression of FMRP fully rescues the *hiw* synaptic growth defect, loss of Dscam1 does not rescue (data not shown). Instead, expression of FMRP phenocopies a loss of Wnd, leading us to test the hypothesis that the Wnd protein levels might be downregulated by dFMRP.

To test if dFMRP decreases Wnd protein levels in the *hiw* mutant nervous system, we used the pan-neuronal driver Elav-GAL4 to overexpress either a control upstream activating sequence (UAS) transgene (RFP) or dFMRP in a *hiw* null background (*hiwΔN*) and measured endogenous Wnd protein levels in the ventral nerve cord (VNC) of third instar larvae. Examination of the VNCs reveals a substantial increase in endogenous Wnd levels in the *hiwΔN* background over wild-type controls, in which Wnd protein is just barely detectable (Figures 1C and 1D). Overexpression of dFMRP in the *hiw* mutant nervous system completely suppresses this increase in Wnd protein in the larval VNC (Figures 1C and 1D), showing that excess dFMRP decreases Wnd protein levels. We next tested whether dFMRP can regulate a transgenic Wnd construct under the control of the exogenous UAS-promoter in *hiw* mutants. Similar to endogenous Wnd, levels of the UAS-Wnd^{KD}GFP transgene are increased in *hiw* mutant VNCs relative to WT—this is completely suppressed by overexpression of dFMRP (Figures 1E and 1F). Hence, dFMRP can regulate Wnd protein levels regardless of whether *wnd* is expressed from the endogenous or exogenous locus and so is unlikely to regulate Wnd levels via a transcriptional mechanism. We conclude that overexpressing dFMRP suppresses *hiw* mutant overgrowth by downregulating Wnd protein levels.

dFMRP Is Required to Limit Wnd Levels in the Nervous System and Interacts with Wnd mRNA

Given that overexpressing dFMRP can negatively regulate Wnd protein levels, we hypothesized that endogenous

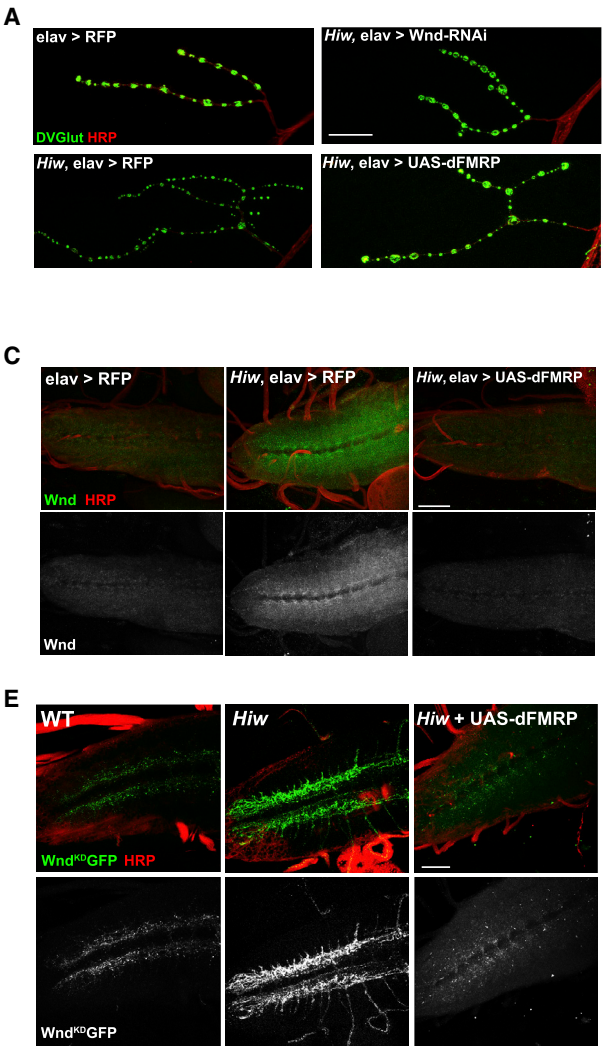

Figure 1. Overexpression of dFMRP Suppresses Synaptic Overgrowth and Decreases Wnd Protein Levels in *hiw* Mutant Larvae

(A) Representative images of the NMJ synaptic terminal at muscle 4 in third-instar larvae. For all genotypes, the pan-neuronal driver Elav-GAL4 was used to express the given transgene, and the wild-type (WT) control is Elav-GAL4 in an otherwise wild-type background driving UAS-RFP. NMJs were stained for the presynaptic bouton marker DVGLUT (green) and nerve membrane marker HRP (red). Scale bar: 25 μm.

(B) Quantification of the mean (±SEM) number of DVGlut+ boutons per muscle 4 NMJ in each genotype. Overexpression of dFMRP completely suppresses NMJ overgrowth in *hiw* mutants.

(C) Representative images of larval ventral nerve cords (VNCs) from wild type (elav > RFP), *hiw* mutants (*hiw* elav > RFP), and *hiw* mutants overexpressing dFMRP (*hiw* elav > dFMRP). VNCs were stained for endogenous Wnd protein (green) and membrane marker HRP (red). Increased Wnd protein levels in *hiw* mutants is suppressed when dFMRP is overexpressed. Scale bar: 50 μm.

(D) Quantification of the mean (±SEM) intensity of Wnd staining in the VNCs for each genotype.

(E) Representative images of larval VNCs from wild type (elav > UAS-Wnd^{KD}GFP), *hiw* (*hiw*,elav > UAS-Wnd^{KD}GFP), and *hiw* overexpressing dFMRP (*hiw*,elav > UAS-Wnd^{KD}GFP,UAS-dFMRP). VNCs were stained for the transgenic Wnd protein using anti-GFP (green) and membrane marker HRP (red). Scale bar: 50 μm.

(F) Quantification of the mean (±SEM) intensity of GFP staining in the VNCs for each genotype.

Statistical tests and exact p values reported in Table S1. *p = 0.05; **p = 0.01; ***p = 0.001; ****p = 0.0001, NS, not significant; p > 0.05.

See also Figure S1.

dFMRP normally regulates Wnd protein levels. To test this, we compared endogenous Wnd protein levels in wild-type VNCs to Wnd levels in two different transheterozygous *dFmr1* mutant backgrounds: the null allele *dFmr1*$^{\Delta 50M}$ (Zhang et al., 2001) over a deficiency line in which *dFmr1* locus is excised (Df(3R)by62 (labeled in Figure 2 as *dFmr1*(1)) and *dFmr1*$^{\Delta 50M}$ over a second null allele, *dFmr1*^{2} (labeled in Figure 2 as *dFmr1*(2); Dockendorff et al., 2002). Western blotting for dFMRP protein confirms that these transheterozygotes lack dFMRP in the nervous system (Figure 2A). Wnd protein levels are significantly increased in the VNCs of *dFmr1* mutants relative to wild type (Figures 2A and 2B). Neuronal expression of a wild-type *dFmr1* rescue transgene (Dockendorff et al., 2002) reverts Wnd protein levels to those of wild-type flies (Figures 2A and 2B). Thus, dFMRP negatively regulates Wnd protein expression in the nervous system, and the absence of dFMRP results in increased Wnd protein.

dFMRP is an RNA binding protein that can stall translation from its target mRNAs. While this is a likely mechanism by which dFMRP is regulating Wnd levels, we sought to test other possible regulatory mechanisms. First, the absence of dFMRP can trigger transcriptional changes (Korb et al., 2017), so we conducted qPCR in wild-type and *dFmr1* larval brains to determine if *wnd* mRNA levels are increased in dFmr1 mutants. We observed no significant difference in *wnd* mRNA in the *dFmr1* nervous system relative to wild type (Figure 2C). Taken with our data that excess dFMRP does not require the endogenous locus to decrease Wnd protein (Figures 1E and 1F), we conclude that dFMRP does not regulate *wnd* at the level of transcription. Second, Wnd protein stability could be increased in *dFmr1* mutants, which could also drive increased Wnd protein levels. We used the protein synthesis inhibitor cycloheximide (CHX) to assess turnover of Wnd protein. Wild-type and *dFmr1* nervous systems were exposed to CHX for 0, 6, 12, and 18 h, and we probed for Wnd protein levels at each time point. As expected, *dFmr1* mutants have higher Wnd protein at baseline (Figure 2D); however, the relative rate of Wnd degradation over the time course did not vary between wild type and *dFmr1* (Figures 2D and 2E), demonstrating that Wnd protein stability is not increased in *dFmr1* mutants.

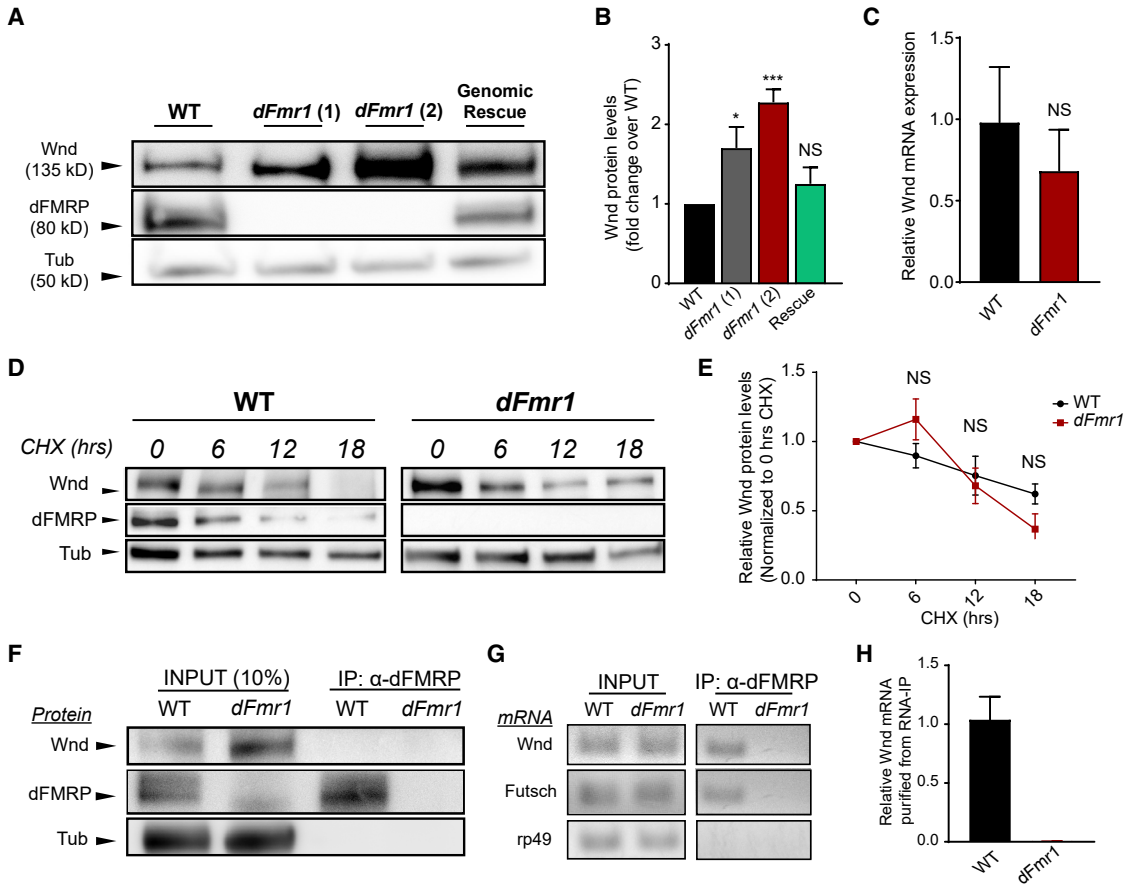

Figure 2. dFMRP Is Required to Limit Wnd Levels in the Nervous System and Binds Wnd mRNA, Suggesting Translational Repression

(A) Representative western blots of Wnd, dFMRP, and Tubulin from larval VNCs taken from wild type, two different *dFmr1*-transheterozygous mutants, and a *dFmr1* transheterozygous mutant with a wild-type *dFmr1* genomic rescue construct inserted on a different chromosome.

(B) Quantification of mean (±SEM) Wnd levels in each genotype. Wnd levels were increased in both *dFmr1* mutants, and the genomic rescue of *dFmr1* abolished the increase.

(C) qPCR quantification of *wnd* mRNA levels in wild-type versus *dFmr1* mutants, presented as fold change relative to wild type. The *wnd* mRNA levels did not differ between wild-type and *dFmr1* mutants.

(D) Representative western blots of wild-type and *dFmr1* mutant larval VNCs after *ex vivo* incubation in cycloheximide (CHX) for the indicated times. Wnd levels are higher at baseline in *dFmr1* mutants, but protein degradation is not inhibited.

(E) Quantification of mean (±SEM) Wnd levels in each genotype at each time point of CHX treatment. Wnd degradation after CHX treatment did not differ between wild-type and *dFmr1* mutants.

(F) Representative immunoblot from wild-type and *dFmr1* mutants. INPUT (left side of blot): 10% of the lysate prior to immunoprecipitation was collected for input controls, and blotting for dFMRP confirms the absence of dFMRP protein in *dFmr1* mutants. IP (right side of the blot): dFMRP protein was immunoprecipitated from *Drosophila* heads, and as expected, no dFMRP was detected from *dFmr1* mutants.

(G) RT-PCR products from input and immunoprecipitated samples from wild-type and *dFmr1* flies. All mRNAs probed (listed on left of image) were present in the RNA input samples extracted from both genotypes. *Futsch* mRNA was used as a positive control and immunoprecipitated with dFMRP. *rp49* mRNA was used as a negative control and did not immunoprecipitate with dFMRP. *wnd* mRNA immunoprecipitated with dFMRP in wild-type flies. No *wnd* mRNA is detected in *dFmr1* mutant immunoprecipitation samples.

(H) qPCR quantification of *wnd* mRNA product detected from immunoprecipitated samples, normalized to *wnd* mRNA from input, and presented as relative mRNA levels compared to wild-type immunoprecipitated *wnd* mRNA. For *dFmr1* mutants, all CT values were >38 or undetectable. All undetectable CT values were set to 40 for the purposes of quantification.

Statistical tests and exact p values reported in Table S1. For all quantifications: *p = 0.05; **p = 0.01; ***p = 0.001; ****p = 0.0001; NS, not significant; p > 0.05.

We then employed RNA immunoprecipitation (RNA-IP) to test the hypothesis that *wnd* is an mRNA target of dFMRP *in vivo* in the fly, which would suggest regulation at the level of translation. We collected lysates from the heads of both wild-type and *dFmr1* null flies and confirmed that dFMRP could be pulled down from wild-type flies, while no dFMRP was present in *dFmr1* mutants (Figure 2F). The pulldowns and subsequent western blots were performed in non-denaturing buffers to preserve any protein-protein interactions between dFMRP and Wnd. We did not detect any Wnd coimmunoprecipitating with dFMRP protein (Figure 2F). We next conducted RT-PCR to assess whether *wnd* mRNA immunoprecipitated with dFMRP.

The mRNA for *Futsch*, a known target of dFMRP in the fly nervous system, was successfully detected in the immunoprecipitated samples from wild-type flies (Figure 2G). Further, the mRNA for *rp49*, a housekeeping gene that is commonly used as a negative control in dFMRP studies (Bienkowski et al., 2017), was not detected in immunoprecipitated samples (Figure 2G). *wnd* mRNA coimmunoprecipitated with dFMRP and can be observed after RT-PCR of the RNA isolated from wild-type samples immunoprecipitated with dFMRP (Figure 2G). The qPCR of immunoprecipitated RNA samples confirmed that *wnd* mRNA is present in wild-type samples and virtually absent in *dFmr1* mutant samples (Figure 2H). Thus, we conclude that dFMRP binds *wnd* mRNA *in vivo*, and Wnd protein is negatively regulated by dFMRP in wild-type animals likely through translational control. These findings are consistent with high-throughput studies conducted in flies and mice that identified both Wnd and DLK, respectively, among FMRP bound transcripts (Darnell et al., 2011; McMahon et al., 2016).

Excess Wnd in the *dFmr1* Mutant Nervous System Drives Defects in Synaptic Morphology

Wnd levels are increased in the *dFmr1* mutant nervous system, and excess Wnd can trigger numerous neuronal phenotypes, including defects in NMJ morphology, axon development, and synaptic physiology (Collins et al., 2006; Goel and Dickman, 2018; Li et al., 2017; Shin and DiAntonio, 2011; Xiong et al., 2010), so we hypothesized that Wnd might be a functionally relevant target required for defects observed in *dFmr1* mutant neurons. *dFmr1* mutant NMJs exhibit well-established morphological phenotypes, with an increase in the number of synaptic boutons that is largely driven by a profusion of satellite boutons, which surround larger boutons rather than occurring individually along the nerve terminal and may represent an arrested state of bouton development (Siller and Broadie, 2011; Zhang et al., 2017; Gatto and Broadie, 2008; Zhang et al., 2001). We first tested if NMJ morphological defects in *dFmr1* mutant larvae are Wnd dependent. We generated double-mutant flies for *dFmr1* and *Wnd* to conduct epistasis analysis of *dFmr1* mutant NMJs. We recombined the $dFmr1^{\Delta 50M}$ and df(*dFmr1*) alleles with two different, previously validated alleles of *wnd*—*wnd-1* and *wnd-3* (Collins et al., 2006)—to generate four unique double-mutant lines in which both dFMRP and Wnd protein are absent. *dFmr1* larvae exhibit synaptic overgrowth with abundant satellite boutons, while *dFmr1*,*Wnd* double mutants do not exhibit increases in total bouton number (Figures 3A and 3B) or in satellite bouton number (Figures 3A and 3C). Larvae mutant for *wnd* alone show no substantial differences in NMJ morphology relative to wild type (Figures 3A–3C). Hence, Wnd is necessary for morphological defects at the *dFmr1* mutant NMJ.

We next asked if Wnd can drive other neuronal morphological defects in *dFmr1* mutants. We have previously demonstrated that *hiw* mutants exhibit Wnd-dependent defects in fly mushroom body (MB) morphology (Shin and DiAntonio, 2011), and MB morphology is also disrupted in *dFmr1* mutants (Michel et al., 2004; Siller and Broadie, 2011). *dFmr1* phenotypes include thin or misprojected α and/or β lobes (Michel et al., 2004). Thus, we tested if dysregulated Wnd also drives MB developmental defects in *dFmr1* mutants. We examined the MBs of wild-type, *dFmr1* mutants, and double *dFmr1*,*Wnd* mutants immediately after eclosion. MB phenotypes are highly sensitive to genetic background (Michel et al., 2004), and in our $dFmr1^{\Delta 50M}$/df(*dFmr1*) adults, the most penetrant phenotype was malformation of the α lobe. The α lobe is substantially thinner than the β lobe, while in wild-type MBs, the width of each lobe is roughly the same (Figures S2A–S2D). We quantified the width of each fly's α and β lobe and present these data as "α/β lobe width ratio" (Figure S2B for schematic; see Method Details for quantification details). The ratio for *dFmr1* MBs is significantly decreased relative to WT (Figure S2C) due to abnormally thin α lobes. After categorizing all the α lobes across genotypes, we found that thin α lobes are a highly penetrant phenotype in mutants, affecting about 80% of the *dFmr1* brains analyzed (Figure S2D). In contrast, there was no significant decrease in the MB lobe width ratio relative to wild type in *dFmr1*,*Wnd* double mutants (Figures S2C and S2D). Hence, Wnd is required for MB lobe malformations in *dFmr1* mutants, demonstrating that the effects of dysregulated Wnd signaling can impact neuronal morphology beyond the larval NMJ.

We returned to the NMJ to assess whether Wnd functions in the neuron to disrupt synaptic development in *dFmr1* mutants. Many important FMRP targets are regulated postsynaptically (Darnell and Klann, 2013); however, the previously described role for Wnd in promoting synaptic growth at the NMJ is presynaptic (Collins et al., 2006). To test this, we employed the pan-neuronal elav-GAL4 driver in a *dFmr1* mutant background to drive an RNAi against Wnd exclusively in neurons. *dFmr1* mutants expressing a control transgene have an increase in the number of synaptic and satellite boutons, compared to a wild-type control (Figures 3D–3F). Presynaptic knockdown of Wnd fully rescued these bouton phenotypes at the larval NMJ (Figures 3D–3F). We next tested if Wnd functions through its canonical MAP kinase cascade, in which the downstream MAP kinase JNK activates the transcription factor Fos (Collins et al., 2006; Xiong et al., 2010), by (1) RNAi knockdown of JNK and (2) overexpression of a dominant-negative transgene for the transcription factor Fos (Fos-DN) in the *dFmr1* mutant background. We observed a complete suppression of the increases in bouton number and the formation of satellite boutons in the *dFmr1* mutant background with either JNK or Fos loss-of-function (Figures 3D–3F). While other MAP3Ks can also signal through JNK and Fos, the full suppression from inhibition of Wnd, JNK, or Fos is consistent with the model that Wnd signaling through a JNK-/Fos-dependent transcriptional program is required for defects in *dFmr1* NMJ synapse morphology.

Excess Wnd in the *dFmr1* Mutant Nervous System Drives Defects in Synaptic Physiology

Having determined that Wnd is necessary in *dFmr1* mutant larval NMJs to drive defects in synaptic terminal morphology, we next sought to determine whether Wnd alters synaptic transmission at the NMJ. Both the fly and mouse models of FXS exhibit significant changes in synaptic transmission (Contractor et al., 2015; Drozd et al., 2018; Repicky and Broadie, 2009). At the larval NMJ in *Drosophila*, previously reported phenotypes include increased evoked release (Zhang et al., 2001) and decreased quantal size (Gatto and Broadie, 2008). We tested if increased

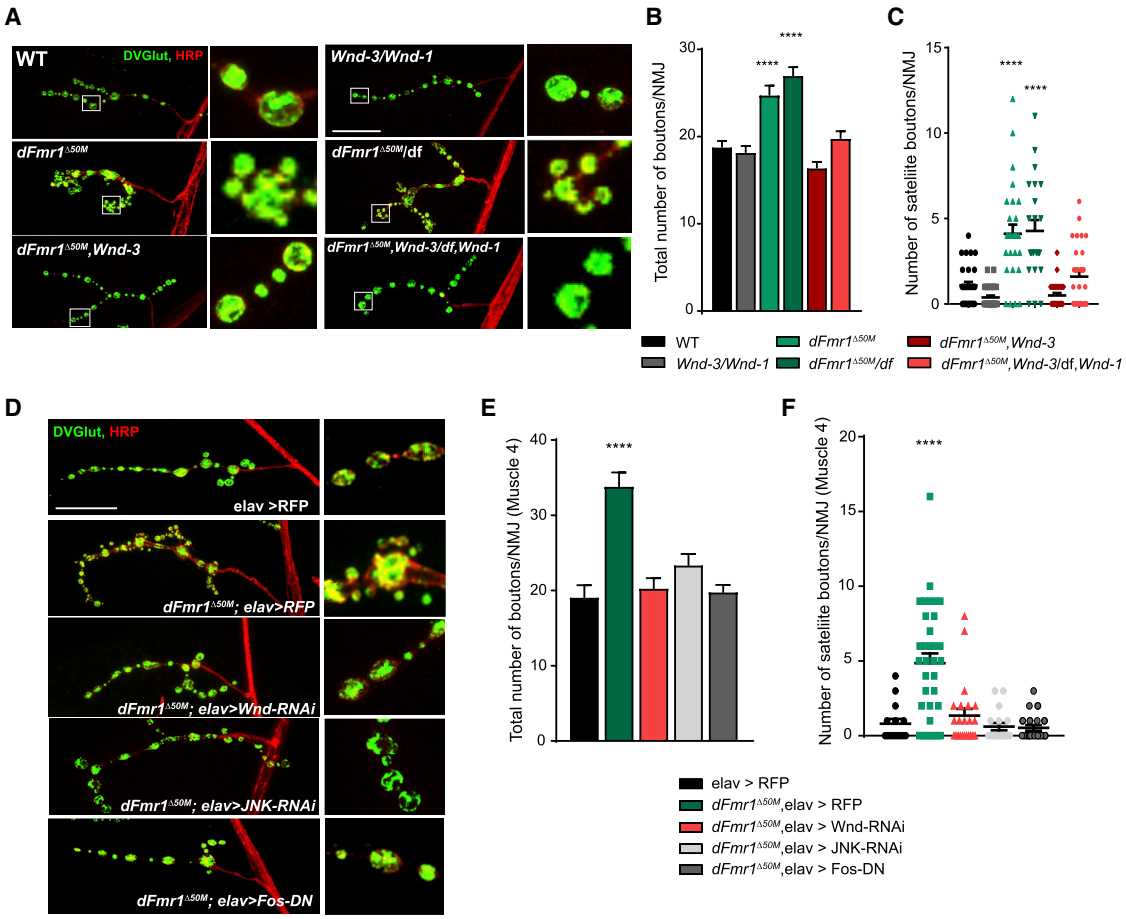

Figure 3. Wnd Is Required for Synaptic Morphology Defects in *dFmr1* Mutants

(A) Representative images of the NMJ synaptic terminal and boutons at muscle 4 in third-instar wild type, Wnd mutant, *dFmr1* mutant, and *dFmr1*,*Wnd* double mutant larvae. NMJs were stained for the presynaptic bouton marker DVGLUT (green) and nerve membrane marker HRP (red). Representative bouton images are shown in the inset panels to the right of the respective genotype.

(B) Quantification of the mean (±SEM) number of boutons per muscle 4 NMJ in each genotype. Total bouton number is increased in *dFmr1* mutants relative to wild type, which is suppressed in *dFmr1,Wnd* double mutants.

(C) Quantification of the mean (±SEM) number of satellite boutons per muscle 4 NMJ in each genotype. Satellite bouton number is increased in dFmr1 mutants relative to wild type, which is suppressed in *dFmr1*,*Wnd* double mutants.

(D) Representative images of the NMJ synaptic terminal and boutons at muscle 4 in third-instar larvae. The Elav-GAL4 driver was used in either a wild-type or *dFmr1* mutant background to drive the respective transgenes. NMJs were stained for the presynaptic bouton marker DVGLUT (green) and nerve membrane marker HRP (red). Representative bouton images are shown in the inset panels to the right of the respective genotype.

(E) Quantification of the mean (±SEM) number of total boutons per muscle 4 NMJ in each genotype.

(F) Quantification of the mean (±SEM) number of satellite boutons per muscle 4 NMJ in each genotype. Suppression by Wnd-RNAi, JNK-RNAi, and Fos-DN for both total and satellite bouton number demonstrates that presynaptic Wnd signaling drives aberrant NMJ morphology in *dFmr1* mutants.

Statistical tests and exact p values reported in Table S1. Scale bar: 25 μm. *p = 0.05; **p = 0.01; ***p = 0.001; ****p = 0.0001; NS, not significant; p > 0.05. See also Figure S2.

Wnd in *dFmr1* mutants leads to changes in synaptic transmission at the larval NMJ. We performed electrophysiological recordings at the larval NMJ of *dFmr1* mutants and observed that relative to wild type, there is an increase in quantal content (Figures 4A and 4D). Notably, and consistent with previous studies, evoked excitatory postsynaptic potential (EPSP) amplitudes are slightly but not significantly increased (Figures 4A and 4B; Repicky and Broadie, 2009). However, the amplitudes of miniature, spontaneous excitatory events (mEPSPs) are significantly decreased in *dFmr1* mutants (Figures 4A and 4C), indicating that increased quantal content is driven by a decrease in postsynaptic response to the neurotransmitter in a single vesicle; thus, the nerve releases more vesicles to compensate for the decreased postsynaptic response. Such homeostatic compensation is well described at the *Drosophila* NMJ (Davis, 2013; Petersen et al., 1997). In *dFmr1*,*Wnd* double mutants, the decrease in mEPSP amplitude is abolished (Figure 4C), and quantal content is restored to wild-type levels (Figure 4D). Neuronal depletion of Wnd via RNAi also suppressed the decrease in mEPSP amplitude and increase in quantal content

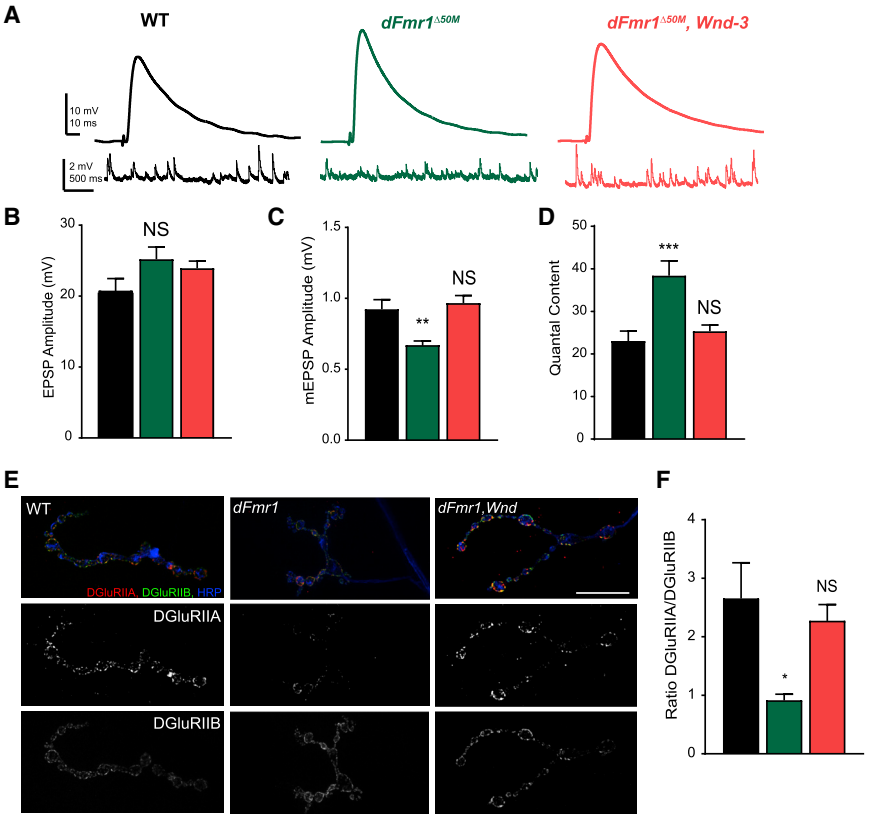

Figure 4. Abnormal Synaptic Transmission at the *dFmr1* Mutant Larval NMJ Requires Wnd

(A) Representative EPSP and mEPSP electrophysiological traces from larval NMJs at Muscle 6 from wild type, *dFmr1* mutant, and double *dFmr1,Wnd* mutants.

(B) Quantification of mean (±SEM) EPSP amplitudes.

(C) Quantification of mean (±SEM) mEPSP amplitudes. Reduced mEPSP amplitude in *dFmr1* mutants is suppressed in *dFmr1,Wnd* double mutants.

(D) Quantification of quantal content, which was calculated individually per cell by dividing the mean EPSP amplitude by the mean mEPSP amplitude, and then averaged per genotype. Increased quantal content in *dFmr1* mutants is abolished in *dFmr1,Wnd* double mutants.

(E) Representative images of wild type, *dFmr1*, and *dFmr1,Wnd* NMJs stained for the glutamate receptor subunits DGluRIIA (red) and DGluRIIB (green). Terminal membrane is stained with HRP (blue). In *dFmr1* larvae, there is a Wnd-dependent decrease in DGluRIIA levels while DGluRIIB levels remained roughly the same.

(F) Quantification of the ratio of DGluRIIA levels to DGluRIIB levels, which was derived from analyzing the fluorescent intensities of each subunit across the entire terminal. *dFmr1* NMJs have a lower DGluRIIA/DGluRIIB ratio, which is suppressed in *dFmr1,Wnd*.

Statistical tests and exact p values reported in Table S1. Scale bar: 10 μm. *p = 0.05; **p = 0.01; ***p = 0.001; ****p = 0.0001; NS, not significant; p > 0.05.

See also Figure S3.

in *dFmr1* mutants (Figures S3A–S3D). Hence, neuronal Wnd is required for the decrease in quantal size and the increase in quantal content during neurotransmission at the *dFmr1* mutant NMJ.

What are the Wnd-dependent mechanisms driving decreased quantal size and increased quantal content at the *dFmr1* mutant synaptic terminal? We first assessed active zones and postsynaptic densities via staining for the active zone protein Bruchpilot (Figures S3E–S3G) and the common glutamate receptor subunit DGluRIII (also known as DGluRIIC; Figures S3E–S3G) and detected no obvious change in levels or localization, suggesting that synapse formation is largely normal in *dFmr1* mutants. We next tested if postsynaptic mechanisms governing sensitivity to neurotransmitters are altered by Wnd. Increased Wnd signaling in the neuron reduces the sensitivity of the postsynaptic muscle via downregulation of glutamate receptors (Goel and Dickman, 2018). Further, dFMRP regulates the ratio of different subclasses of ionotropic glutamate receptor subunits at the larval NMJ (Pan and Broadie, 2007; Tessier and Broadie, 2012), and we have previously shown that the ratio of the two alternative subunits, DGluRIIA and DGluRIIB, regulates quantal size (DiAntonio et al., 1999). Thus, we tested if excess Wnd is driving changes in glutamate receptor subunit expression in *dFmr1* mutants. We observed that the ratio of DGluRIIA to DGluRIIB expression is decreased in *dFmr1* mutants in a Wnd-dependent manner (Figures 4E and 4F). Less DGluRIIA decreases quantal size (DiAntonio et al., 1999), so this would explain the decreased mEPSP amplitudes in *dFmr1* mutants. Taken together, these findings indicate that changes in synaptic transmission at the NMJ in *dFmr1* mutants are due to increased neuronal Wnd signaling altering postsynaptic glutamate receptor subunit composition.

dFmr1 Mutant Repetitive Grooming Behaviors are Wnd Dependent

Both *Drosophila* and mammalian models of FXS display behavioral abnormalities (Drozd et al., 2018). Given that Wnd is a critical downstream target of dFMRP in neuronal development and synaptic physiology, we sought to determine if this regulatory relationship extends beyond nervous system development and is required for normal behavior in *Drosophila* adults. One known *dFmr1* mutant behavioral phenotype is excessive, repetitive grooming (Tauber et al., 2011). Adult flies execute stereotyped exploratory behavior when introduced into a novel chamber, alternating between bouts of walking, stopping, and grooming (Phillis et al., 1993; Soibam et al., 2013). *dFmr1* mutants groom excessively, spending significantly more total time grooming and more time in each bout of grooming than do wild-type flies. This grooming phenotype emerges as flies age (Tauber et al., 2011). Adapting a previously published assay (Figure 5A; Tauber et al., 2011), we tested if *dFmr1,Wnd* double mutants retain this defect in grooming. We observed that wild-type and *dFmr1*

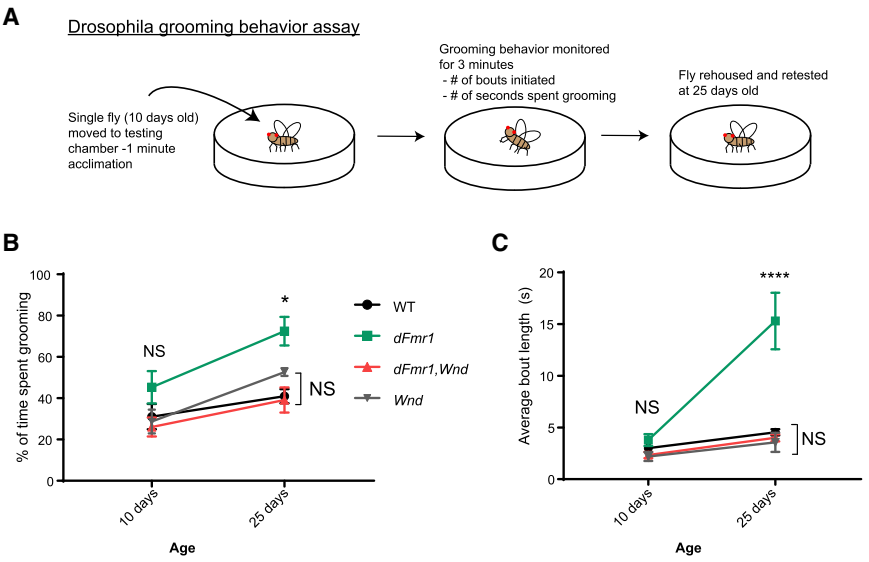

Figure 5. *dFmr1* Mutant Repetitive Grooming Behaviors Are Wnd Dependent

(A) Illustration depicting experimental setup and timeline to assay adult *Drosophila* grooming behavior. For all genotypes, flies were tested at 10 and 25 days to assess grooming duration and grooming bout length. All analysis was performed blinded to genotype and in random order.

(B) Quantification of percent of time spent grooming during a 3-min trial. There were no significant differences among wild-type, *Wnd*, or *dFmr1,Wnd* double mutants at any age.

(C) Quantification of average bout length within each 3-min trial at each age. There were no significant differences among wild-type, *Wnd*, or *dFmr1,Wnd* double mutants at any age.

*p = 0.05; **p = 0.01; ***p = 0.001; ****p = 0.0001; NS, not significant; p > 0.05. p values shown on figure represent statistical comparison to wild-type control within the same testing age.

Detailed statistical tests and additional comparisons available in Table S1.

mutant flies groom the same amount at 10 days of age, but by day 25, grooming in wild-type flies remains stable while *dFmr1* mutants groom themselves excessively (Figures 5B and 5C; Videos S1, S2, and S3). Excitingly, *dFmr1,Wnd* double mutants did not display any excessive grooming activity and were statistically indistinguishable from wild type at both ages tested (Figures 5B and 5C; Videos S1, S2, and S3). *wnd* mutants alone did not show any repetitive grooming behaviors (Figures 5B and 5C). Thus, Wnd is necessary for the excessive grooming behavior of *dFmr1* mutant flies.

A Chemical Inhibitor of Wnd Suppresses NMJ Defects in *dFmr1* Mutant Larvae

The genetic data demonstrate that increased Wnd drives various neurological phenotypes in *dFmr1* mutant larvae and flies. If excess Wnd signaling drives defects in *dFmr1* mutants, then inhibiting the kinase activity of Wnd should also suppress *dFmr1*-dependent defects. Potent and selective kinase inhibitors of DLK, the mammalian ortholog of Wnd, block DLK-dependent neurodegenerative phenotypes (Patel et al., 2017; Pichon et al., 2017; Summers et al., 2018). We tested whether this DLK inhibitor (DLKi) can inhibit Wnd signaling. The most potent and best-described Wnd-dependent phenotype in *Drosophila* is the synaptic terminal overgrowth in *hiw* mutants, so we raised *hiw* mutant larvae on food dosed with the DLK inhibitor and assessed synaptic terminal morphology. In the *hiw* mutant, synaptic terminal overgrowth was fully suppressed when the larvae consumed DLK inhibitor-dosed food, while wild-type larvae raised on DLK inhibitor had no change in synaptic growth (Figures 6A and 6B). Thus, the DLK inhibitor suppresses the *hiw* NMJ phenotype, a downstream readout of increased Wnd MAP kinase signaling, as robustly as does genetic loss of *wnd* (Collins et al., 2006). Hence, we conclude that the DLK inhibitor is an effective inhibitor of the Wnd kinase in *Drosophila*. We next raised *dFmr1* mutants on the DLK inhibitor and analyzed synaptic morphology. As with the *hiw* mutant, the DLK inhibitor suppresses aberrant synaptic morphology in *dFmr1* mutant larvae (Figures 6C–6E). The *dFmr1* mutants raised on the DLK inhibitor do not exhibit an increase in total or satellite boutons relative to wild type, while *dFmr1* mutants raised on the vehicle retain these defects (Figures 6C–6E). Thus, pharmacological inhibition of Wnd kinase signaling can suppress synaptic development defects in the *Drosophila* FXS model.

Feeding Adult *dFmr1* Mutant Flies the DLK Inhibitor Blocks Repetitive Grooming Behaviors

The ultimate goal in developing therapies for FXS is to ameliorate the symptoms associated with the disorder. Given that the DLK inhibitor treatment suppresses synaptic development abnormalities in *dFmr1* mutant larvae, we tested if treatment with the DLK inhibitor could block excessive grooming behavior in *dFmr1* mutant flies. Since the behavioral defects could result from prior developmental defects, we first asked if treating developing larvae with the DLK inhibitor would suppress behavioral defects in adults. Larvae remained on the DLK inhibitor from embryonic stage through pupation, and flies were moved to regular food within 8 h of eclosion. Grooming behavior was observed and quantified on days 10 and 25 post-eclosion. Developmental treatment with the DLK inhibitor did not reverse defects in grooming behavior. *dFmr1* mutants raised as larvae on either the DMSO or DLK inhibitor displayed excessive grooming activities at day 25 relative to wild type (Figures 7A and 7B). We next asked if treating adult *dFmr1* mutant flies with the DLK inhibitor, after larval and pupal development has occurred, is sufficient to block excessive grooming. Larvae were raised on regular food, and within 8 h of eclosion, adult flies to be tested for grooming were moved onto food dosed with the DMSO or DLK inhibitor and were examined for grooming behavior at days 10 and 25. Excitingly, feeding adult flies the DLK inhibitor is sufficient to prevent excessive grooming behavior in the *dFmr1* mutants (Figures 7C and 7D). This suggests that aberrant Wnd signaling persists beyond development, and the deleterious effects of this signaling promotes excessive grooming behavior. Thus, Wnd signaling can be pharmacologically targeted to restore normal behavior to *dFmr1* mutants,

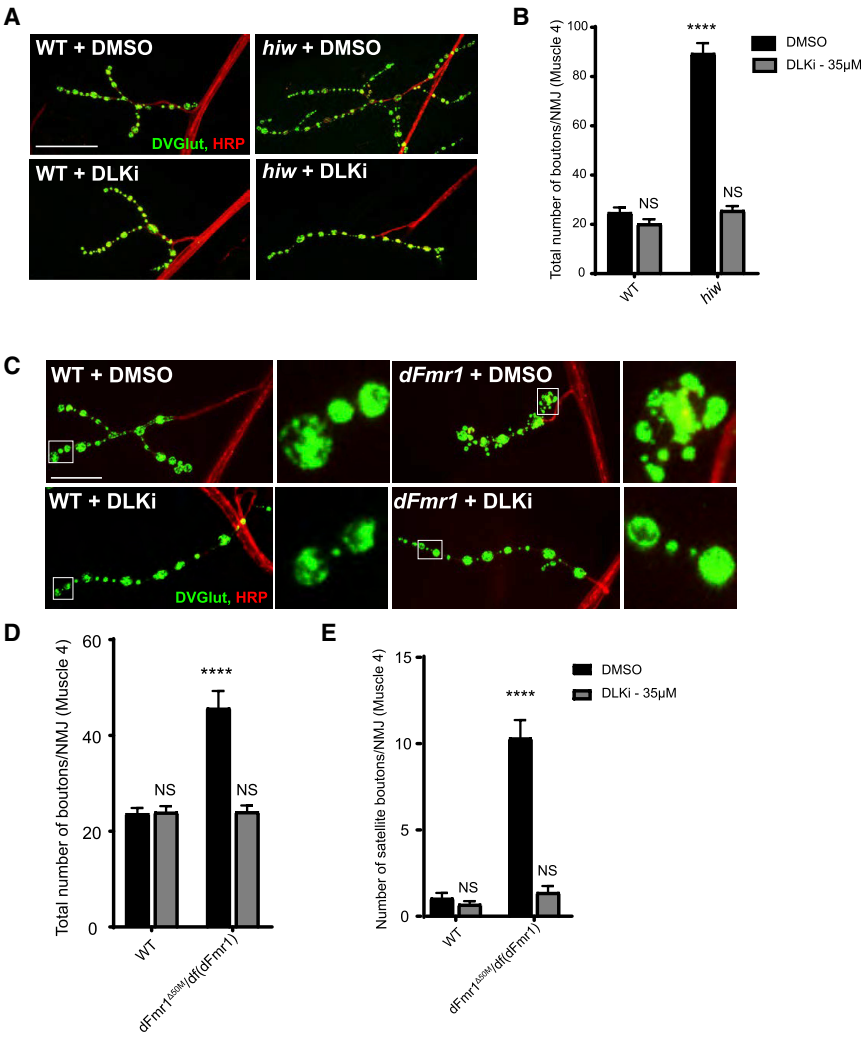

Figure 6. An Inhibitor Against the Mammalian Ortholog of Wnd, DLK, Suppresses NMJ Morphology Defects in *dFmr1* Mutant Larvae

(A) Representative images of the NMJ synaptic terminal at muscle 4 in third-instar wild-type and *hiw* mutant larvae raised on food treated with either DMSO (vehicle control) or DLK inhibitor (DLKi). NMJs were stained for the presynaptic bouton marker DVGLUT (green) and nerve membrane marker HRP (red). Scale bar: 50 μm.

(B) Quantification of the mean (±SEM) number of boutons per muscle 4 NMJ in each genotype in each treatment condition. Feeding the DLK inhibitor to larvae is sufficient to suppress Wnd-dependent *hiw* synaptic overgrowth.

(C) Representative images of the NMJ synaptic terminal at muscle 4 in third-instar wild-type and *dFmr1* mutant larvae raised on food treated with either DMSO (vehicle control) or DLK inhibitor. Representative bouton images are shown in the inset panels to the right of the respective genotype. Scale bar: 25 μm.

(D) Quantification of the mean (±SEM) number of total boutons per muscle 4 NMJ in each genotype in each treatment condition.

(E) Quantification of the mean (±SEM) number of satellite boutons per muscle 4 NMJ in each genotype. Feeding the DLK inhibitor to dFmr1 larvae is sufficient to suppress increases in total and satellite bouton number.

*p = 0.05; **p = 0.01; ***p = 0.001; ****p = 0.0001; NS, not significant; p > 0.05. p values shown on figure represent statistical comparison to wild type treated with DMSO.

Detailed statistical tests and additional comparisons available in Table S1.

even after the bulk of neuronal development is complete, highlighting the possibility of targeting the Wnd/DLK signaling cascade for therapeutic intervention in FXS.

DISCUSSION

FXS is a common and pervasive neurodevelopmental disorder for which there are no effective therapeutic strategies. Here, we demonstrate that the highly conserved MAP3K Wnd is dysregulated in the *Drosophila* model of FXS. *wnd* is an mRNA target of dFMRP in the fly nervous system, and Wnd protein levels are elevated in *dFmr1* mutants. Genetic depletion of *wnd* in larvae and adults lacking dFMRP suppresses aberrant neuronal morphology, physiology, and behavioral defects. Further, larvae and adults can be orally dosed with an inhibitor against the mammalian ortholog of Wnd to suppress NMJ development and adult behavioral defects. We conclude that aberrant Wnd signaling through its canonical MAP kinase cascade drives a wide variety of neurological defects imparted by the loss of dFMRP. This work highlights Wnd/DLK inhibition as a possible therapeutic strategy for FXS.

FMRP: One RNA Binding Protein, Many Targets

The search for a single, key target of FMRP that could be leveraged to alleviate the symptoms of FXS has been challenging and has yet to yield a viable therapeutic strategy (Erickson et al., 2017; Lee et al., 2018). This is perhaps not surprising, given that FMRP regulates a large set of target mRNAs, and the respective protein products have roles in virtually every aspect of neuronal function, including synaptic development and transmission (Ascano et al., 2012; Darnell et al., 2011). Moreover, loss of FMRP drives defects in many biological processes, including basal translation (Banerjee et al., 2018), epigenetic modification (Korb et al., 2017), metabolism (Weisz et al., 2018), and excitability (Contractor et al., 2015). As such, it was a surprising and exciting result that Wnd/DLK behaves as an essential, functionally relevant target for many of the neuronal phenotypes in the *Drosophila* model of FXS.

Why might overactive Wnd/DLK signaling have such a profound impact on FXS? Activation of Wnd/DLK triggers wide-ranging effects throughout the neuron, including defects in the synapse, axon, and cell body. As a MAP3K, Wnd phosphorylates downstream MAP kinases that both signal locally and activate a

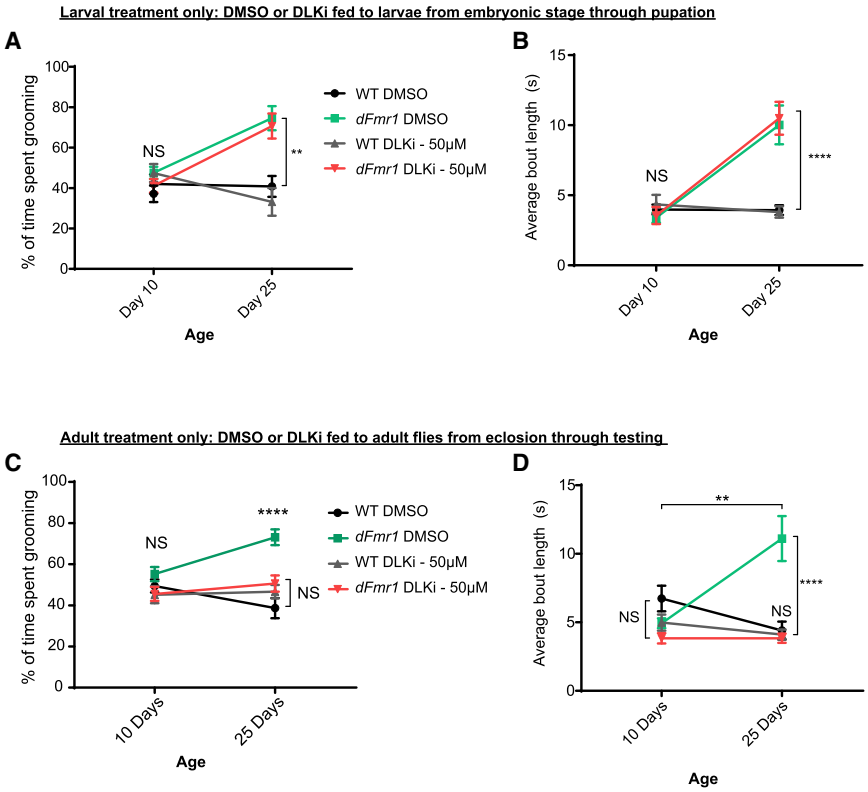

Figure 7. Feeding DLK Inhibitor to *dFmr1* Mutant Adult Flies Prevents Repetitive Grooming Behavior

(A) Wild-type and dFmr1 mutant larvae were raised from embryonic stages through pupation on food dosed with either vehicle (DMSO) or DLK inhibitor (50 uM). Adult flies were immediately moved to regular food after eclosion and consumed regular food throughout adulthood. Quantification of percent of time spent grooming during 3-min trials on days 10 and 25. *dFmr1* mutants exhibited increased grooming in both conditions.

(B) Quantification of average bout length within each 3-min trial for wild-type and *dFmr1* flies raised as larvae on either DMSO or DLK inhibitor. Average bout length was calculated by dividing the total number of bouts initiated by the total number of seconds spent grooming.

(C) Wild-type and dFmr1 mutant larvae were raised from embryonic stages through pupation on normal food, and adult flies were moved to food dosed with either DMSO or DLK inhibitor within 8 h of eclosion, limiting treatment to post-development. Quantification of percent of time spent grooming during a 3-min trial for wild-type and *dFmr1* adult flies treated with either DMSO or DLK inhibitor post-eclosion.

(D) Quantification of average bout length within each 3-minute trial for wild-type and *dFmr1* flies treated with either DMSO or DLK inhibitor post-eclosion. Feeding DLK inhibitor to dFmr1 mutant adults was sufficient to prevent repetitive grooming.

*p = 0.05; **p = 0.01; ***p = 0.001; ****p = 0.0001; NS, not significant; p > 0.05. p values shown on figure represent statistical comparison to wild-type control within the same testing age unless noted by an additional bar.

Detailed statistical tests and additional comparisons available in Table S1.

major transcriptional response governing critical cell stress pathways. We posit that reduction of Wnd/DLK signaling has such profound effects in suppressing *dFmr1* mutant phenotypes because the consequences of Wnd activation are not limited to a single pathway or cellular compartment. Of course, other FMRP targets also must contribute to neuronal dysfunction, and overactive Wnd/DLK signaling likely interacts with these other dysregulated proteins. Indeed, increased Wnd/DLK signaling in *dFmr1* mutants and *hiw* mutants yields very different synaptic phenotypes, suggesting that the impact of Wnd/DLK activation is influenced by other molecular abnormalities in the *dFmr1* mutants. It will be critical in future studies to understand how downstream effectors of Wnd/DLK signaling interact with other dysregulated molecular pathways to govern the numerous neurological defects apparent in models of FXS.

DLK Signaling in Injury and Disease

Wnd/DLK signaling through its canonical MAP kinase cascade is a critical feature of the neuronal response to insult and injury. In acute axon injury paradigms, Wnd/DLK promotes distal axon degeneration by speeding up the turnover of axon survival factors (Summers et al., 2018; Walker et al., 2017). In the proximal axon, Wnd/DLK stimulates a retrograde signal to the neuronal cell body that can stimulate axon regeneration or neuronal cell death depending on the cell type (Shin et al., 2012; Watkins et al., 2013; Welsbie et al., 2013). This retrograde signal involves activation of the MAP kinase JNK and phosphorylation of the transcription factor Jun to mount the appropriate transcriptional response. In addition to responding to acute injury, there is emerging evidence that Wnd/DLK is chronically activated in neurodegenerative diseases. DLK and JNK signaling is active in both mouse models of and human patients with Alzheimer's disease and amyotrophic lateral sclerosis (Pichon et al., 2017). The loss or inhibition of DLK protects against the progressive neuronal degeneration that occurs in these mouse models, paralleling our finding that progressive worsening of repetitive behaviors in the *dFmr1* fly can be reversed by the DLK inhibitor. We hypothesize that low-level, chronic activation of Wnd/DLK signaling might be a shared feature of neurodevelopmental and neurodegenerative disorders. Indeed, it is estimated that 50%–70% of people with Down syndrome develop Alzheimer's disease (Hartley et al., 2015; Head et al., 2012), and premutations in the *Fmr1* gene can cause the neurodegenerative disorder fragile X-associated tremor/ataxia syndrome (Hagerman and Hagerman, 2013), so a critical link may exist between development and degeneration.

Wnd/DLK as a Candidate Therapeutic Target in FXS

FXS is characterized by neuroanatomical and functional defects that are established during development, leading to lifelong

cognitive, sensory, and behavioral abnormalities. However, from our work in the fly model of FXS, we propose that the key factors underlying this neurodevelopmental disorder can be parsed into two stages: neuronal development is disrupted by increased Wnd/DLK signaling, and aberrant Wnd/DLK signaling persists throughout the lifetime of the organism, further impairing neuronal function. This model is consistent with prior studies of FMRP-regulated processes, including metabotropic glutamate receptor (mGluR)-dependent protein translation (Dölen et al., 2007; Hou et al., 2006; Huber et al., 2002). mGluR activation stimulates protein translation in dendritic spines, and normally FMRP inhibits translation to serve as a ''brake''; the absence of FMRP leads to excessive translation of synaptic proteins and increased AMPA receptor internalization, driving synaptic dysfunction (Dölen and Bear, 2008; Muddashetty et al., 2007; Stoppel et al., 2017). Thus, not only is initial development impaired due to improper levels of specific synaptic proteins, but increased flux through mGluR-dependent translational mechanisms drive ongoing perturbations to synaptic plasticity and function. This concept, which has made downregulation of mGluR signaling an attractive treatment approach, is critical when considering Wnd/DLK as a therapeutic target in FXS—there are signaling abnormalities that can be alleviated through inhibition of Wnd/DLK's kinase function even after development is complete.

The idea of targeting Wnd/DLK for treatment in FXS has other advantages. First, Wnd/DLK is a MAP3K with numerous downstream signaling effectors; if DLK inhibition does not lend itself well to therapeutic inhibition, further examination of the signaling cascade may identify alternative approaches and targets. Second, while DLK is essential for embryonic development, conditional knockout of DLK later in life does not impact viability (Miller et al., 2009), suggesting that DLK inhibition is a reasonable therapeutic strategy. Finally, highly selective inhibitors against DLK are currently being tested in patients as treatments for neurodegenerative disorders (Siu et al., 2018). Testing whether the FMRP-dependent regulation of DLK is conserved and functionally relevant in the mouse model of FXS is imperative, and positive results in such experiments may motivate additional translational studies.

STAR★METHODS

Detailed methods are provided in the online version of this paper and include the following:

- KEY RESOURCES TABLE
- LEAD CONTACT AND MATERIALS AVAILABILITY
- EXPERIMENTAL MODEL AND SUBJECT DETAILS
  - *Drosophila* Rearing, Strains, and Genetics
- METHOD DETAILS
  - Immunocytochemistry
  - Western Blots
  - Cycloheximide Chase
  - qPCR
  - RNA Immunoprecipitation
  - Electrophysiology
  - Imaging and Image Analysis
  - DLK Inhibitor Experiments
  - Grooming behavior
- QUANTIFICATION AND STATISTICAL ANALYSIS
- DATA AND CODE AVAILABILITY

SUPPLEMENTAL INFORMATION

Supplemental Information can be found online at https://doi.org/10.1016/j.celrep.2019.08.001.

ACKNOWLEDGMENTS

This work was supported by funding from the NIH grants R01 NS065053 and R01 CA219866 to A.D. and NIH F31 NS101827 to A.R. We thank Thomas Jongens for sharing *dFmr1* flies. We thank Joe Dougherty and the Dougherty lab for technical advice and assistance. We also thank Jeff Milbrandt and the Milbrandt lab for helpful discussions. Lastly, we are grateful to all members of the DiAntonio Lab for fruitful scientific discussions and support.

AUTHOR CONTRIBUTIONS

A.R. and A.D. designed the research, A.R. performed the research and analyzed data, and A.R and A.D. wrote the paper.

DECLARATION OF INTERESTS

The authors declare no competing interests.

Received: February 22, 2019
Revised: July 2, 2019
Accepted: July 30, 2019
Published: September 3, 2019

REFERENCES

Ascano, M., Jr., Mukherjee, N., Bandaru, P., Miller, J.B., Nusbaum, J.D., Corcoran, D.L., Langlois, C., Munschauer, M., Dewell, S., Hafner, M., et al. (2012). FMRP targets distinct mRNA sequence elements to regulate protein expression. Nature *492*, 382–386.

Asghari Adib, E., Smithson, L.J., and Collins, C.A. (2018). An axonal stress response pathway: degenerative and regenerative signaling by DLK. Curr. Opin. Neurobiol. *53*, 110–119.

Ashley, C., Jr., Wilkinson, K.D., Reines, D., and Warren, S.T. (1993). FMR1 protein: conserved RNP family domains and selective RNA binding. Science *262*, 563–566.

Bailey, D.B., Jr., Hatton, D.D., Mesibov, G., Ament, N., and Skinner, M. (2000). Early development, temperament, and functional impairment in autism and fragile X syndrome. J. Autism Dev. Disord. *30*, 49–59.

Banerjee, A., Ifrim, M.F., Valdez, A.N., Raj, N., and Bassell, G.J. (2018). Aberrant RNA translation in fragile X syndrome: From FMRP mechanisms to emerging therapeutic strategies. Brain Res. *1693* (*Pt A*), 24–36.

Bardoni, B., and Mandel, J.-L. (2002). Advances in understanding of fragile X pathogenesis and FMRP function, and in identification of X linked mental retardation genes. Curr. Opin. Genet. Dev. *12*, 284–293.

Bassell, G.J., and Warren, S.T. (2008). Fragile X syndrome: loss of local mRNA regulation alters synaptic development and function. Neuron *60*, 201–214.

Berry-Kravis, E., Raspa, M., Loggin-Hester, L., Bishop, E., Holiday, D., and Bailey, D.B. (2010). Seizures in fragile X syndrome: characteristics and comorbid diagnoses. Am. J. Intellect. Dev. Disabil. *115*, 461–472.

Bhogal, B., and Jongens, T.A. (2010). Fragile X syndrome and model organisms: identifying potential routes of therapeutic intervention. Dis. Model. Mech. *3*, 693–700.

Bienkowski, R.S., Banerjee, A., Rounds, J.C., Rha, J., Omotade, O.F., Gross, C., Morris, K.J., Leung, S.W., Pak, C., Jones, S.K., et al. (2017). The conserved,

disease-associated RNA binding protein dNab2 interacts with the Fragile-X protein ortholog in Drosophila neurons. Cell Rep. *20*, 1372–1384.

Brace, E.J., Wu, C., Valakh, V., and DiAntonio, A. (2014). SkpA restrains synaptic terminal growth during development and promotes axonal degeneration following injury. J. Neurosci. *34*, 8398–8410.

Brown, V., Jin, P., Ceman, S., Darnell, J.C., O'Donnell, W.T., Tenenbaum, S.A., Jin, X., Feng, Y., Wilkinson, K.D., Keene, J.D., et al. (2001). Microarray identification of FMRP-associated brain mRNAs and altered mRNA translational profiles in fragile X syndrome. Cell *107*, 477–487.

Coffee, R.L., Jr., Tessier, C.R., Woodruff, E.A., 3rd, and Broadie, K. (2010). Fragile X mental retardation protein has a unique, evolutionarily conserved neuronal function not shared with FXR1P or FXR2P. Dis. Model. Mech. *3*, 471–485.

Collins, C.A., Wairkar, Y.P., Johnson, S.L., and DiAntonio, A. (2006). Highwire restrains synaptic growth by attenuating a MAP kinase signal. Neuron *51*, 57–69.

Comery, T.A., Harris, J.B., Willems, P.J., Oostra, B.A., Irwin, S.A., Weiler, I.J., and Greenough, W.T. (1997). Abnormal dendritic spines in fragile X knockout mice: maturation and pruning deficits. Proc. Natl. Acad. Sci. USA *94*, 5401–5404.

Contractor, A., Klyachko, V.A., and Portera-Cailliau, C. (2015). Altered Neuronal and Circuit Excitability in Fragile X Syndrome. Neuron *87*, 699–715.

Crawford, D.C., Acuña, J.M., and Sherman, S.L. (2001). FMR1 and the fragile X syndrome: human genome epidemiology review. Genet. Med. *3*, 359–371.

Daniels, R.W., Collins, C.A., Gelfand, M.V., Dant, J., Brooks, E.S., Krantz, D.E., and DiAntonio, A. (2004). Increased expression of the Drosophila vesicular glutamate transporter leads to excess glutamate release and a compensatory decrease in quantal content. J. Neurosci. *24*, 10466–10474.

Daniels, R.W., Gelfand, M.V., Collins, C.A., and DiAntonio, A. (2008). Visualizing glutamatergic cell bodies and synapses in Drosophila larval and adult CNS. J. Comp. Neurol. *508*, 131–152.

Darnell, J.C., and Klann, E. (2013). The translation of translational control by FMRP: therapeutic targets for FXS. Nat. Neurosci. *16*, 1530–1536.

Darnell, J.C., Van Driesche, S.J., Zhang, C., Hung, K.Y.S., Mele, A., Fraser, C.E., Stone, E.F., Chen, C., Fak, J.J., Chi, S.W., et al. (2011). FMRP stalls ribosomal translocation on mRNAs linked to synaptic function and autism. Cell *146*, 247–261.

Davis, G.W. (2013). Homeostatic signaling and the stabilization of neural function. Neuron *80*, 718–728.

DiAntonio, A., Petersen, S.A., Heckmann, M., and Goodman, C.S. (1999). Glutamate receptor expression regulates quantal size and quantal content at the Drosophila neuromuscular junction. J. Neurosci. *19*, 3023–3032.

Dickman, D.K., Lu, Z., Meinertzhagen, I.A., and Schwarz, T.L. (2006). Altered synaptic development and active zone spacing in endocytosis mutants. Curr. Biol. *16*, 591–598.

Dockendorff, T.C., Su, H.S., McBride, S.M.J., Yang, Z., Choi, C.H., Siwicki, K.K., Sehgal, A., and Jongens, T.A. (2002). Drosophila lacking dfmr1 activity show defects in circadian output and fail to maintain courtship interest. Neuron *34*, 973–984.

Dölen, G., and Bear, M.F. (2008). Role for metabotropic glutamate receptor 5 (mGluR5) in the pathogenesis of fragile X syndrome. J. Physiol. *586*, 1503–1508.

Dölen, G., Osterweil, E., Rao, B.S.S., Smith, G.B., Auerbach, B.D., Chattarji, S., and Bear, M.F. (2007). Correction of fragile X syndrome in mice. Neuron *56*, 955–962.

Drozd, M., Bardoni, B., and Capovilla, M. (2018). Modeling Fragile X Syndrome in *Drosophila*. Front. Mol. Neurosci. *11*, 124.

Erickson, C.A., Davenport, M.H., Schaefer, T.L., Wink, L.K., Pedapati, E.V., Sweeney, J.A., Fitzpatrick, S.E., Brown, W.T., Budimirovic, D., Hagerman, R.J., et al. (2017). Fragile X targeted pharmacotherapy: lessons learned and future directions. J. Neurodev. Disord. *9*, 7.

Feng, Y., Ueda, A., and Wu, C.-F. (2004). A modified minimal hemolymph-like solution, HL3.1, for physiological recordings at the neuromuscular junctions of normal and mutant *Drosophila* larvae. J. Neurogenet. *18*, 377–402.

Gatto, C.L., and Broadie, K. (2008). Temporal requirements of the fragile X mental retardation protein in the regulation of synaptic structure. Development *135*, 2637–2648.

Gerdts, J., Summers, D.W., Milbrandt, J., and DiAntonio, A. (2016). Axon self-destruction: new links among SARM1, MAPKs, and NAD+ metabolism. Neuron *89*, 449–460.

Goel, P., and Dickman, D. (2018). Distinct homeostatic modulations stabilize reduced postsynaptic receptivity in response to presynaptic DLK signaling. Nat. Commun. *9*, 1856.

Hagerman, R., and Hagerman, P. (2013). Advances in clinical and molecular understanding of the FMR1 premutation and fragile X-associated tremor/ataxia syndrome. Lancet Neurol. *12*, 786–798.

Hartley, D., Blumenthal, T., Carrillo, M., DiPaolo, G., Esralew, L., Gardiner, K., Granholm, A.-C., Iqbal, K., Krams, M., Lemere, C., et al. (2015). Down syndrome and Alzheimer's disease: Common pathways, common goals. Alzheimers Dement. *11*, 700–709.

Head, E., Powell, D., Gold, B.T., and Schmitt, F.A. (2012). Alzheimer's Disease in Down Syndrome. Eur. J. Neurodegener. Dis. *1*, 353–364.

Hou, L., Antion, M.D., Hu, D., Spencer, C.M., Paylor, R., and Klann, E. (2006). Dynamic translational and proteasomal regulation of fragile X mental retardation protein controls mGluR-dependent long-term depression. Neuron *51*, 441–454.

Huber, K.M., Gallagher, S.M., Warren, S.T., and Bear, M.F. (2002). Altered synaptic plasticity in a mouse model of fragile X mental retardation. Proc. Natl. Acad. Sci. USA *99*, 7746–7750.

Kim, J.H., Wang, X., Coolon, R., and Ye, B. (2013). Dscam expression levels determine presynaptic arbor sizes in Drosophila sensory neurons. Neuron *78*, 827–838.

Korb, E., Herre, M., Zucker-Scharff, I., Gresack, J., Allis, C.D., and Darnell, R.B. (2017). Excess Translation of Epigenetic Regulators Contributes to Fragile X Syndrome and Is Alleviated by Brd4 Inhibition. Cell *170*, 1209–1223.e20.

Lee, J., and Wu, C.-F. (2010). Orchestration of stepwise synaptic growth by K+ and Ca2+ channels in Drosophila. J. Neurosci. *30*, 15821–15833.

Lee, A.W., Ventola, P., Budimirovic, D., Berry-Kravis, E., and Visootsak, J. (2018). Clinical Development of Targeted Fragile X Syndrome Treatments: An Industry Perspective. Brain Sci. *8*, E214.

Li, J., Zhang, Y.V., Adib, E.A., Stanchev, D.T., Xiong, X., Klinedinst, S., Soppina, P., Jahn, T.R., Hume, R.I., Rasse, T.M., et al. (2017). Restraint of presynaptic protein levels by Wnd/DLK signaling mediates synaptic defects associated with the kinesin-3 motor Unc-104. eLife *6*, e24271.

Marrus, S.B., Portman, S.L., Allen, M.J., Moffat, K.G., and DiAntonio, A. (2004). Differential localization of glutamate receptor subunits at the Drosophila neuromuscular junction. J. Neurosci. *24*, 1406–1415.

McMahon, A.C., Rahman, R., Jin, H., Shen, J.L., Fieldsend, A., Luo, W., and Rosbash, M. (2016). TRIBE: Hijacking an RNA-Editing Enzyme to Identify Cell-Specific Targets of RNA-Binding Proteins. Cell *165*, 742–753.

Michel, C.I., Kraft, R., and Restifo, L.L. (2004). Defective neuronal development in the mushroom bodies of Drosophila fragile X mental retardation 1 mutants. J. Neurosci. *24*, 5798–5809.

Miller, B.R., Press, C., Daniels, R.W., Sasaki, Y., Milbrandt, J., and DiAntonio, A. (2009). A dual leucine kinase-dependent axon self-destruction program promotes Wallerian degeneration. Nat. Neurosci. *12*, 387–389.

Muddashetty, R.S., Kelić, S., Gross, C., Xu, M., and Bassell, G.J. (2007). Dysregulated metabotropic glutamate receptor-dependent translation of AMPA receptor and postsynaptic density-95 mRNAs at synapses in a mouse model of fragile X syndrome. J. Neurosci. *27*, 5338–5348.

Pan, L., and Broadie, K.S. (2007). Drosophila fragile X mental retardation protein and metabotropic glutamate receptor A convergently regulate the synaptic ratio of ionotropic glutamate receptor subclasses. J. Neurosci. *27*, 12378–12389.

Patel, S., Meilandt, W.J., Erickson, R.I., Chen, J., Deshmukh, G., Estrada, A.A., Fuji, R.N., Gibbons, P., Gustafson, A., Harris, S.F., et al. (2017). Selective Inhibitors of Dual Leucine Zipper Kinase (DLK, MAP3K12) with Activity in a Model of Alzheimer's Disease. J. Med. Chem. *60*, 8083–8102.

Petersen, S.A., Fetter, R.D., Noordermeer, J.N., Goodman, C.S., and DiAntonio, A. (1997). Genetic analysis of glutamate receptors in Drosophila reveals a retrograde signal regulating presynaptic transmitter release. Neuron *19*, 1237–1248.

Phillis, R.W., Bramlage, A.T., Wotus, C., Whittaker, A., Gramates, L.S., Seppala, D., Farahanchi, F., Caruccio, P., and Murphey, R.K. (1993). Isolation of mutations affecting neural circuitry required for grooming behavior in Drosophila melanogaster. Genetics *133*, 581–592.

Pichon, C.E.L., Meilandt, W.J., Dominguez, S., Solanoy, H., Lin, H., Ngu, H., Gogineni, A., Ghosh, A.S., Jiang, Z., Lee, S.-H., et al. (2017). Loss of dual leucine zipper kinase signaling is protective in animal models of neurodegenerative disease. Sci. Transl. Med. *9*, eaag0394.

Pieretti, M., Zhang, F.P., Fu, Y.-H., Warren, S.T., Oostra, B.A., Caskey, C.T., and Nelson, D.L. (1991). Absence of expression of the FMR-1 gene in fragile X syndrome. Cell *66*, 817–822.

Repicky, S., and Broadie, K. (2009). Metabotropic glutamate receptor-mediated use-dependent down-regulation of synaptic excitability involves the fragile X mental retardation protein. J. Neurophysiol. *101*, 672–687.

Schneider, C.A., Rasband, W.S., and Eliceiri, K.W. (2012). NIH Image to ImageJ: 25 years of image analysis. Nat. Methods *9*, 671–675.

Shin, J.E., and DiAntonio, A. (2011). Highwire regulates guidance of sister axons in the Drosophila mushroom body. J. Neurosci. *31*, 17689–17700.

Shin, J.E., Cho, Y., Beirowski, B., Milbrandt, J., Cavalli, V., and DiAntonio, A. (2012). Dual leucine zipper kinase is required for retrograde injury signaling and axonal regeneration. Neuron *74*, 1015–1022.

Siller, S.S., and Broadie, K. (2011). Neural circuit architecture defects in a Drosophila model of Fragile X syndrome are alleviated by minocycline treatment and genetic removal of matrix metalloproteinase. Dis. Model. Mech. *4*, 673–685.

Simon, D.J., and Watkins, T.A. (2018). Therapeutic opportunities and pitfalls in the treatment of axon degeneration. Curr. Opin. Neurol. *31*, 693–701.

Siu, M., Sengupta Ghosh, A., and Lewcock, J.W. (2018). Dual Leucine Zipper Kinase Inhibitors for the Treatment of Neurodegeneration. J. Med. Chem. *61*, 8078–8087.

Soibam, B., Shah, S., Gunaratne, G.H., and Roman, G.W. (2013). Modeling novelty habituation during exploratory activity in Drosophila. Behav. Processes *97*, 63–75.

Stoppel, L.J., Auerbach, B.D., Senter, R.K., Preza, A.R., Lefkowitz, R.J., and Bear, M.F. (2017). β-arrestin2 couples metabotropic glutamate receptor 5 to neuronal protein synthesis and is a potential target to treat fragile X. Cell Rep. *18*, 2807–2814.

Summers, D.W., Milbrandt, J., and DiAntonio, A. (2018). Palmitoylation enables MAPK-dependent proteostasis of axon survival factors. Proc. Natl. Acad. Sci. USA *115*, E8746–E8754.

Tauber, J.M., Vanlandingham, P.A., and Zhang, B. (2011). Elevated levels of the vesicular monoamine transporter and a novel repetitive behavior in the Drosophila model of fragile X syndrome. PLoS ONE *6*, e27100.

Tessier, C.R., and Broadie, K. (2012). Molecular and genetic analysis of the Drosophila model of fragile X syndrome. Results Probl. Cell Differ. *54*, 119–156.

The Dutch-Belgian Fragile X Consortium (1994). Fmr1 knockout mice: a model to study fragile X mental retardation. Cell *78*, 23–33.

Walker, L.J., Summers, D.W., Sasaki, Y., Brace, E.J., Milbrandt, J., and DiAntonio, A. (2017). MAPK signaling promotes axonal degeneration by speeding the turnover of the axonal maintenance factor NMNAT2. eLife *6*, e22540.

Wan, H.I., DiAntonio, A., Fetter, R.D., Bergstrom, K., Strauss, R., and Goodman, C.S. (2000a). Highwire regulates synaptic growth in Drosophila. Neuron *26*, 313–329.

Wan, L., Dockendorff, T.C., Jongens, T.A., and Dreyfuss, G. (2000b). Characterization of dFMR1, a Drosophila melanogaster homolog of the fragile X mental retardation protein. Mol. Cell. Biol. *20*, 8536–8547.

Wang, H. (2015). Fragile X mental retardation protein: from autism to neurodegenerative disease. Front. Cell. Neurosci. *9*, 43.

Warren, S.T., and Nelson, D.L. (1994). Advances in molecular analysis of fragile X syndrome. JAMA *271*, 536–542.

Watkins, T.A., Wang, B., Huntwork-Rodriguez, S., Yang, J., Jiang, Z., Eastham-Anderson, J., Modrusan, Z., Kaminker, J.S., Tessier-Lavigne, M., and Lewcock, J.W. (2013). DLK initiates a transcriptional program that couples apoptotic and regenerative responses to axonal injury. Proc. Natl. Acad. Sci. USA *110*, 4039–4044.

Weisz, E.D., Towheed, A., Monyak, R.E., Toth, M.S., Wallace, D.C., and Jongens, T.A. (2018). Loss of Drosophila FMRP leads to alterations in energy metabolism and mitochondrial function. Hum. Mol. Genet. *27*, 95–106.

Welsbie, D.S., Yang, Z., Ge, Y., Mitchell, K.L., Zhou, X., Martin, S.E., Berlinicke, C.A., Hackler, L., Jr., Fuller, J., Fu, J., et al. (2013). Functional genomic screening identifies dual leucine zipper kinase as a key mediator of retinal ganglion cell death. Proc. Natl. Acad. Sci. USA *110*, 4045–4050.

Wu, C., Wairkar, Y.P., Collins, C.A., and DiAntonio, A. (2005). Highwire function at the Drosophila neuromuscular junction: spatial, structural, and temporal requirements. J. Neurosci. *25*, 9557–9566.

Xiong, X., Wang, X., Ewanek, R., Bhat, P., Diantonio, A., and Collins, C.A. (2010). Protein turnover of the Wallenda/DLK kinase regulates a retrograde response to axonal injury. J. Cell Biol. *191*, 211–223.

Yao, K.-M., and White, K. (1994). Neural specificity of elav expression: defining a Drosophila promoter for directing expression to the nervous system. J. Neurochem. *63*, 41–51.

Zhang, Y.Q., Bailey, A.M., Matthies, H.J.G., Renden, R.B., Smith, M.A., Speese, S.D., Rubin, G.M., and Broadie, K. (2001). Drosophila fragile X-related gene regulates the MAP1B homolog Futsch to control synaptic structure and function. Cell *107*, 591–603.

Zhang, X.-Y., Qi, J., Shen, Y.-Q., Liu, X., Liu, A., Zhou, Z., Han, J., and Zhang, Z.C. (2017). Mutations of PQBP1 in Renpenning syndrome promote ubiquitin-mediated degradation of FMRP and cause synaptic dysfunction. Hum. Mol. Genet. *26*, 955–968.

STAR★METHODS

KEY RESOURCES TABLE

REAGENT or RESOURCE	SOURCE	IDENTIFIER
Antibodies		
Rabbit anti-DVGLUT	DiAntonio Lab	RRID: AB_2314346
Rabbit anti-dGluRIII	DiAntonio Lab	N/A
Mouse anti-DGluRIIA	Developmental Studies Hybridoma Bank (DSHB)	DSHB Cat# 8B4D2 (MH2B); RRID: AB_528269
Rabbit anti-DGluRIIB	DiAntonio Lab	N/A
Mouse anti-Bruchpilot	DSHB	DSHB Cat# NC82; RRID: AB_2314866
Mouse anti-Fasicilin II	DSHB	Cat# 1D4; RRID: AB_528235
Rabbit anti-Wallenda	DiAntonio Lab	N/A
Cy3 goat anti-HRP	Jackson ImmunoResearch	Cat# 123-165-021; RRID: AB_2338959
647 goat anti-HRP	Jackson ImmunoResearch	Cat# 123-605-021; RRID: AB_2338967
AlexaFluor 488 goat anti-GFP	ThermoScientific - Invitrogen	Cat# A-21311; RRID: AB_221477
AlexaFluor 488 goat anti-rabbit	ThermoScientific – Invitrogen	Cat# A-11034; RRID: AB_2576217
Cy3 goat anti-mouse	Jackson ImmunoResearch	Cat# 115-165-146; RRID: AB_2338680
Mouse anti-dFMRP	DSHB	Cat#5B6; RRID: AB_528253
Mouse anti-beta tubulin	DSHB	Cat# E7; RRID: AB_2315513
Chemicals, Peptides, and Recombinant Proteins		
Cycloheximide	Santa Cruz Biotechnology	Cat# Sc-3508
Trizol	ThermoFisher	Cat# 15596018
DNase	Sigma-Aldrich	Cat# DN25-1G
qScript cDNA synthesis kit	VWR, QuantaBio	Cat# 101414-098
PerfeCTa SYBR Green FastMix - Rox	VWR, QuantaBio	Cat# 101414-278
Protease inhibitor – cOmplete mini EDTA-free	SigmaAldrich	Cat# 11836170001
RNase inhibitor - RNAsin	ThermoFischer Scientific	Cat# PRN2615
DLK inhibitor – GNE-3511	MedChem Express	Cat# HY-12947
Formula 4-24 Instant Drosophila Medium Blue Food	Carolina Biological Supply	Cat# 173210
Critical Commercial Assays		
Pierce Protein Micro BCA Assay	ThermoFischer Scientific	Cat# 23227
Protein G Dynabeads	ThermoFischer Scientific	Cat# 10003D
Experimental Models: Organisms/Strains		
hiw$^{\Delta N}$	DiAntonio Lab	RRID: BDSC_51637
hiw^{ND8}	DiAntonio Lab	RRID: BDSC_51638
Wnd-1	DiAntonio Lab	RRID: BDSC_51641
Wnd-3	DiAntonio Lab	RRID: BDSC_51999
DVGlut-Gal4	DiAntonio Lab	N/A
elav3E-Gal4	DiAntonio Lab	N/A
dFmr1^{2}	Jongens Lab	N/A
WTR;*dFmr1*^{3}	Jongens Lab	N/A
dFmr1$^{\Delta 50M}$,*wnd-3*	This paper	N/A
dFmr1(df),wnd-1	This paper	N/A
UAS-RFP	Bloomington Drosophila Stock Center (BDSC)	#32218
Df(3R)Exel6265 (dFmr1(df))	BDSC	#7732
dFmr1$^{\Delta 50M}$	BDSC	#6930
UAS-dFMRP	BDSC	#6931

(*Continued on next page*)

Continued		
REAGENT or RESOURCE	SOURCE	IDENTIFIER
UAS-JNK-RNAi	BDSC	#57035
UAS-Fos^{DN}	BDSC	#7214
UAS-wallenda-RNAi	BDSC	#25396
Oligonucleotides		
Primers for *rp49, wnd, and futsch,* see STAR Methods	This paper	N/A
Software and Algorithms		
ImageJ	Schneider et al., 2012	https://imagej.nih.gov/ij/
MiniAnalysis	Synaptosoft	N/A
pClamp9	Molecular Devices	N/A
Prism	GraphPad Software	N/A

LEAD CONTACT AND MATERIALS AVAILABILITY

Further information and requests for resources and reagents should be directed to and will be fulfilled by the Lead Contact, Aaron DiAntonio (diantonio@wustl.edu). The double *dFmr1,Wnd* mutant fly strains generated in this study are available upon request. No other unique reagents were generated in this study.

EXPERIMENTAL MODEL AND SUBJECT DETAILS

Drosophila Rearing, Strains, and Genetics

Drosophila were cultured employing standard techniques, and all crosses were maintained at 25°C in 60% relative humidity. The following stocks were used in this study: *hiw*$^{\Delta N}$ (null allele of *hiw*; Wu et al., 2005), *hiw*^{ND8} (strong hypomorphic allele of *hiw*; Wan et al., 2000a), *wnd-1* and *wnd-3* (Collins et al., 2006), DVGlut-Gal4 (Daniels et al., 2008), elav3E-Gal4 (Yao and White, 1994), *dFmr1*^{2} (a gift from Thomas Jongens), WTR;*dFmr1*^{3} (a gift from Thomas Jongens) (Dockendorff et al., 2002). Flies obtained from the Bloomington Stock Center included: UAS-RFP (#32218), UAS-wallenda-RNAi (TRiP Collection #25396), UAS-dFMRP (#6931), *dFmr1*$^{\Delta 50M}$ (#6930; Zhang et al., 2001), Df(3R)Exel6265 (#7732, deficiency line for *dFmr1*), UAS-JNK-RNAi (#57035), and UAS-Fos^{DN} (#7214).

In all experiments in which a GAL4 driver was employed, control larvae were generated by crossing virgins of the respective driver used to UAS-RFP males. Roughly equal numbers of male and female larvae and flies were tested (with the exception of *hiw* mutants, in which only males were assessed as *hiw* is on the X chromosome), and no sex-specific differences were observed in any experiment. Detailed genotypic information for each experiment is available in Table S1.

Standard techniques were used for recombination of the *dFmr1* and *wnd* mutant alleles. All double mutants generated via recombination were tested for the presence of the respective mutant alleles via PCR, followed by western blots to verify the absence of protein product.

METHOD DETAILS

Immunocytochemistry

NMJs and VNCs: Third instar larvae were dissected in either cold PBS or Ca^{2+}-free HL3 and fixed in either Bouin's fixative for 10 min at RT or for 20 min in ice cold 4% paraformaldehyde. After fixing, larval preps were washed in PBS + 0.1% Triton X-100 (PBST), then blocked and stained in PBST + 5% goat serum. Larvae were incubated overnight in primary antibodies, including rabbit α-DVGLUT antibody (1:5000; Daniels et al., 2004), rabbit α-DGluRIII (1:1000; Marrus et al., 2004), mouse α-DGluRIIA (8B4D2, 1:100, Developmental Studies Hybridoma Bank), rabbit α-DGluRIIB (1:500; Marrus et al., 2004), mouse α-Brp (NC82, 1:100, Developmental Studies Hybridoma Bank) and rabbit α-Wallenda antibody (Collins et al., 2006) at 1:600 dilution. After incubation with primary, larvae were washed in PBST and incubated for 1 hour in the following secondary antibodies: Cy3 and 649-conjugated goat α-HRP (1:1000, Jackson ImmunoResearch), AlexaFluor 488-conjugated α-rabbit (1:1000, Invitrogen), AlexaFluor 488-conjugated α-GFP (1:1000, Invitrogen), and Cy3 α-mouse (1:1000, Jackson ImmunoResearch). After secondary, larval preps were equilibrated in 70% glycerol in PBS, and mounted and imaged in Vectashield (Vector Laboratories).

Mushroom bodies: Within 12 hours of eclosion, adult flies were anesthetized on ice and decapitated with forceps. The brain was dissected and removed in cold PBS and fixed for 20 minutes in ice cold 4% paraformaldehyde. After fixing, brains were gently washed 3 times in PBS, and then washed in PBS + 0.1% Triton X-100 (PBST), then blocked overnight in PBST + 5% goat serum, rotating at 4°C. Brains were then incubated for at least 48 hours in primary antibody (mouse anti-FasII, Developmental Studies

Hybridoma Bank, 1:5 dilution in block) rotating at 4°C. Brains were then washed three times in PBST for 10 minutes, and incubated in secondary antibody (Cy3 α-mouse) for 3 hours, rotating at room temperature. After secondary, brains were washed in PBS, and equilibrated directly in Vectashield for at least 2 hours at 4°C. Brains were then mounted and imaged.

Western Blots

To analyze protein levels in the third instar larval nervous system, ventral nerve cords (VNCs) were dissected and homogenized on ice in lysis buffer (100 mM NaCl, 100 mM Tris ph 8.0, 1 mM EDTA pH 8.0, 2 M urea, 1% v/v SDS, 20 mM Na3VO4, 1x Roche protease inhibitor) with a pestle. VNCs from 10 genetically identical flies were pooled into one lysate to achieve sufficient protein concentration, and the lysate was boiled for 10 minutes, and centrifuged at RT for 10 minutes at 13000 RPM. Gel electrophoresis and transfer were performed by standard procedures (Wu et al., 2005). Membranes were blocked for 1 hour and incubated overnight at 4°C in primary antibody solution consisting of 5% milk solution in Tris-buffered saline with 0.2% Tween-20 (TBST), and one of the following antibodies: rabbit α-Wallenda (1:800), mouse α-dFMRP (5B6, Developmental Studies Hybridoma Bank, 1:500), and mouse β-Tubulin (E7, Developmental Studies Hybridoma Bank, 1:100). Primary antibody solution was removed, membranes were washed 3 times with TBST, and membranes were then incubated with HRP conjugated secondary antibodies to either anti-mouse or anti-rabbit antibody (Jackson, 1:10,000). After 1 hr of incubation, membranes were washed 3 times for 10 minutes in TBST, 1 time for 10 minutes in TBS, and developed using Immobilon Western Chemiluminescent Substrate (EMD Millipore). Membranes were imaged on a G:Box Chemi-XX6 (Syngene) and quantified using ImageJ. Wnd band intensities were normalized to the intensity of their respective β-Tubulin loading control band, and intensities are represented as fold change over the control genotype.

Cycloheximide Chase

To measure Wnd protein stability, an *ex vivo* preparation was employed to expose the intact nervous system to cycloheximide (CHX) for varying periods of time. Briefly, third instar larvae were dissected in ice-cold HL3.1. Upon exposure of the nervous system tissue and removal of gut tissue, dissected larvae were incubated in CHX (100 μg/mL) dissolved in HL3.1 for 6, 12, or 18 hours. After the indicated time, VNCs were dissected out and transferred to an Eppendorf tube, residual HL3.1 + CHX was removed with a pipette, and ice cold lysis buffer (described above) was added to VNC samples. 0hr time point samples were collected from VNCs after dissection in normal HL3.1. Samples were homogenized in lysis buffer, and a Micro BCA Assay was used to measure total protein and ensure equal loading across conditions and genotypes. Wnd, dFMRP, and Tub protein levels were measured and analyzed employing the western blot protocol described above. 8 to 10 VNCs were pooled per time point per genotype for each biological replicate of the CHX experiment, and 3 independent biological replicates were completed and are represented in the quantification. For each time point, Wnd protein intensities were normalized to levels of the loading control (Tub), and these values were normalized to the 0hr time point for the given genotype to present relative changes in Wnd levels over time.

qPCR

5 ventral nerve cords were dissected in ice cold PBS and incubated for 5 minutes followed by homogenization in Trizol, and the manufacturer's instructions were followed to extract RNA. After nanodropping for concentration and DNase treatment (Promega) to eliminate genomic DNA, First-strand cDNA synthesis was performed using Quanta Biosciences qScript cDNA synthesis kit according to manufacturer's instructions. cDNA was diluted for quantitative RT-PCR with Quanta Biosciences PerfeCTa SYBR Green FastMix with Rox. Data were analyzed using the ΔΔCT Method to calculate *wnd* mRNA fold change between WT and *dFmr1* mutants. Quantification represents 5 biologically independent replicates. *wnd* mRNA levels were normalized to levels of the housekeeping gene *rp49*. The following primers were used to probe for *rp49* (housekeeping control) and *wnd*:

rp49 forward TACAGGCCCAAGATCGTGAAG
rp49 reverse GACGCACTCTGTTGTCGATACC
wnd forward GGCAGGCTAAAGAACGAGACT
wnd reverse CCAAGCGGGACGGTAACAT

RNA Immunoprecipitation

Sample preparation and immunoprecipitation: ~200 adult fly heads were collected and homogenized in 750 uL ice cold lysis buffer (50 mM Tris-HCL pH 7.4, 10 mM NaCl, 1% NP-40, 10mM Na_3VO_4, and 10mM NaF) with 1X protease inhibitors (Sigma-Aldrich, cOmplete mini EDTA-free, #11836170001) and RNase inhibitor (RNAsin, 1U/μL, Thermo Fischer Scientific, #PRN2615). Homogenized lysate was spun at 4°C for 30 minutes and the pellet was discarded, and 500 uL of supernatant was collected. 50 uL of supernatant was collected and saved for Input blots. Protein G Dynabeads (Thermo Fischer Scientific, #10003D) were coupled to anti-dFMRP (Developmental Studies Hybridoma Bank, 25 μg antibody per 40 uL beads) by rotating end over end for 2 hours at RT. The remaining 450 uL of supernatant was precleared with blank beads for 1 hour rotating at RT. The supernatant was then transferred to tubes containing the Dynabeads conjugated to dFMRP antibody, and tubes were rotated overnight at 4°C. The following day, the beads were collected, washed 5 times for 1 minute each in a high-salt wash buffer (50 mM Tris-HCl pH 7.4, 350 mM NaCl, 1% NP-40, and 1 U/ μL RNAsin), and resuspended in 200 uL of lysis buffer. 50 uL was collected and processed for western blot to assess immunoprecipitation of dFMRP, and 150 uL was added to 100 uL of PBS and 750 uL Trizol to be processed for RNA extraction.

RNA extraction and qRT-PCR: Beads conjugated to the dFMRP protein were processed with Trizol following the manufacturer's instructions (ThermoFisher Scientific, #15596026) to isolate mRNA species bound to dFMRP. Isolated RNA was Nanodropped to acquire RNA concentration, and then equal amounts of RNA from each genotype was treated with DNase (Sigma-Aldrich, DN25-1G) and cDNA was synthesized following the manufacturer's instructions (qScript cDNA Synthesis Kit, Quantabio, VWR #733-1177). To probe for and amplify the presence of sequences of interest, qPCR was conducted on the cDNA purified from the dFMRP-bead complex, and the primer sequences for *wnd* and *rp49* are the same as described above, and the primer sequences for *Futsch* (positive control for association with dFMRP) were:

Futsch forward ATCACCGCAAGTTTTGAAGG
Futsch reverse GCGAAGTCTTTTGGTGCTTC

To generate representative gel images, qPCR products were run on a 2% agarose gel and imaged using G:Box Chemi-XX6 (Syngene). Images are representative of 3 independently conducted RNA-immunoprecipitation experiments in which the results were indistinguishable.

Electrophysiology

Intracellular recordings were performed as described previously (Daniels et al., 2004). In brief, wandering 3rd instar larvae were dissected in Ca^{2+} free HL3.1 buffer (Feng et al., 2004) (70 mm NaCl, 5 mm KCl, 8 mm MgCl2, 10 mm NaHCO3, 5 mm trehalose, 5 mm HEPES, and 0 mm Ca^{2+}, pH 7.2) and then washed with and recorded in HL3.1 buffer containing 0.35 mM Ca^{2+}. Spontaneous mEPSPs and evoked EPSPs were recorded from muscle 6 in segments A2, A3, and A4 using borosilicate sharp electrodes (15–20 MΩ). Intracellular recordings were only used if a resting membrane potential between −60 and −80 mV could be maintained through the duration of the recording and if the muscle input resistance was > 5 MΩ. We did not observe significant differences in resting membrane potential or input resistance between genotypes in any experiment. 75 consecutive spontaneous events were measured per cell using MiniAnalysis Software (Synaptosoft, Decatur, GA) to determine mEPSP mean amplitude and frequency. Evoked EPSPs were recorded by sucking the end of a cut segmental nerve into a stimulating electrode and stimulating with a 1 ms pulse of sufficient amperage to recruit both axons innervating muscle 6. EPSP amplitude was calculated by averaging 75 consecutive evoked events at 2 Hz using pClamp9 software (Molecular Devices). Quantal content (QC) for each individual cell was estimated by dividing the average EPSP amplitude by the average mEPSP amplitude.

Imaging and Image Analysis

To assess synaptic growth, larvae stained for DVGlut and HRP were imaged using a 40x-oil or 63x-oil immersion objective on a Leica TCS SPE confocal microscope. Images shown are maximal Z-projections of confocal stacks. Images for a given experiment (including experiments described below) were taken simultaneously using identical laser power, gain, and offset settings using the same step-size. Synaptic growth was quantified as previously described (Brace et al., 2014; Collins et al., 2006). Briefly, DVGlut-positive boutons were manually counted at larval muscle 4, segments A2 through A4, from at least 4 larvae per genotype. For Figures 3 and 6, both the total number of boutons and the number of satellite boutons were collected during counting. Satellite boutons were defined as boutons that were 1) smaller in size than immediately adjacent boutons and 2) emerging from an adjacent bouton rather than being spaced along a section of HRP positive nerve (Dickman et al., 2006; Lee and Wu, 2010).

To assess Wnd levels, larval ventral nerve cords were imaged using a 20x-oil immersion objective. Wnd levels were measured by analyzing confocal stacks for fluorescence intensity using ImageJ software (NIH; Schneider et al., 2012). A mask was created using the HRP channel to select the entire area encompassed by nervous system membrane. The mask was then applied to the stacks in which the Wnd channel had been isolated, and the mean intensity for the entire area was acquired. Mean Wnd/GFP intensities were normalized to the total area of the VNC compartment, and then presented as the fold change over the WT (control) intensity.

To assess levels of synaptic proteins (Brp, DGluRIII, DGluRIIA, DGluRIIB), NMJs were imaged using a 63x-oil immersion objective, and confocal stacks were collected and analyzed for fluorescence intensity using ImageJ software (NIH). A mask was created using the HRP channel to select the entire synaptic terminal area, and the mask was applied to stacks in which the channel of interest had been isolated. The mean intensity for the entire area was acquired, normalized to the total area of the synaptic terminal, and presented as either 1) the ratio of expression of receptor subunits, found by dividing the mean DGluRIIA intensity by the mean DGluRIIB intensity (Figure 4F) or 2) the mean intensity of the given protein (Brp and DGluRIII) across the entire terminal in arbitrary units (Figures S3F and S3G).

To quantify mushroom body phenotypes in adult fly brains, mushroom body structures were imaged using a 20x-oil immersion objective. ImageJ software was used to measure the α and β lobe widths for each individual mushroom body. Using these data, an α/β lobe width ratio was calculated by dividing the α lobe width by the β lobe width for each individual mushroom body, and the average ratio for each genotype is presented. As the mushroom body is a symmetrical paired structure, each brain contains a set of two α lobes and two β lobes, both of which were quantified in each brain. Thus, each brain contributed an N of 2, with lobes exhibiting damage from the dissection being excluded from analyses. To calculate the percent penetrance of thin α lobe phenotypes, we defined "thin α lobe" as an α lobe with a width that was less than the WT mean width minus two-standard deviations. α lobes that met this criterion were classified as "thin," and counted toward the percent of lobes exhibiting the thin phenotype.

DLK Inhibitor Experiments

GNE-3511 (MedChem Express HY-12947) referred to as DLKi, was resuspended from powder into 10 mM aliquots in DMSO. To dose larvae or flies with DLKi, the drug was diluted to either 35 uM (larvae) or 50 uM (adults) in the appropriate quantity of water to add to Formula 4-24 Instant *Drosophila* Medium Blue Food (Carolina, #173210) to make enough food to fill the bottom of an empty vial. For larval experiments, crosses were made directly on Blue Food such that egg-laying took place on food dosed with either control (DMSO in water) or DLKi, and larvae were exposed to drugged food for the entirety of development until dissection. For adults, flies were collected within 8 hours of eclosion and moved immediately to Blue Food with either control or DLKi. Adult flies were moved onto fresh Blue Food with the respective treatment every 5 days to ensure the drug remained active.

Grooming behavior

Grooming behaviors were observed and analyzed as previously described (Tauber et al., 2011). Briefly, male and female virgin flies of each genotype and/or drug condition were collected within 8 hours of eclosion and housed on either regular food (for genetic experiments in Figure 5 and larval dosing experiments in Figure 6) or Blue Food prepared and dosed with either drug vehicle (DMSO) or DLKi at 50 uM. 12 hours prior to testing, flies were lightly anesthetized on ice and housed individually and moved to the behavioral testing room. On the testing day, each individual fly was gently tapped into a testing chamber comprised of a small clear plastic Petri dish with an agar coated bottom. After one minute of acclimation to the chamber, grooming behaviors were observed for 3 minutes. A stopwatch was used to record the duration of grooming activities and count the number of grooming bouts initiated. After the trial, flies were rehoused on the appropriate medium. Flies were tested at days 10 and 25 post-eclosion. No significant differences in grooming were observed between male and female flies from the same genotype at any age or treatment, thus all data presented are from roughly equal numbers of male and female flies.

QUANTIFICATION AND STATISTICAL ANALYSIS

For all NMJ immunostaining and electrophysiological experiments, each NMJ terminal is considered an *N* of 1 since each presynaptic motor neuron is confined to its own muscle hemisegment. To control for variability between larvae within a genotype in these experiments, all data were collected from a minimum of 4 different larvae. With the exception of *hiw* experiments, in which only males were assessed because *hiw* is on the X chromosome, male and female larvae were used in equal numbers and it was confirmed that there are no statistical differences in NMJ morphology or physiology between males and females. For Wnd intensity experiments, each VNC contributed an *N* of 1.

In all immunostaining (larval and adult) experiments, animals were dissected and the data were analyzed blinded to genotype, and genotype was only decoded after the analysis was complete. For electrophysiology, the experimenter was blinded to genotype while recording and genotypes were decoded after traces were analyzed. For behavior, experimenter was blinded to genotype and condition, and individual flies were observed for grooming in random order, with each individual trial for each fly contributing an *N* of 1. Genotypes and conditions were decoded after the experiments were complete.

For all biochemistry experiments (Western blots and RNA-IP), each experiment was repeated at least three times with larvae and/or flies derived from independently made crosses. Each lane was loaded with protein from a pooled sample of 8-10 VNCs for a given genotype and experiment, and each experiment was independently conducted at least 3 times.

All data are presented as mean ± SEM. Detailed information on exact statistical tests used, N for each experiment, and exact p values can be found in Table S1, including additional statistical comparisons of interest that are not presented within the figures.

DATA AND CODE AVAILABILITY

This study did not generate or analyze datasets or code.

Cell Reports, Volume *28*

Supplemental Information

Wnd/DLK Is a Critical Target of FMRP Responsible for Neurodevelopmental and Behavior Defects in the *Drosophila* Model of Fragile X Syndrome

Alexandra Russo and Aaron DiAntonio

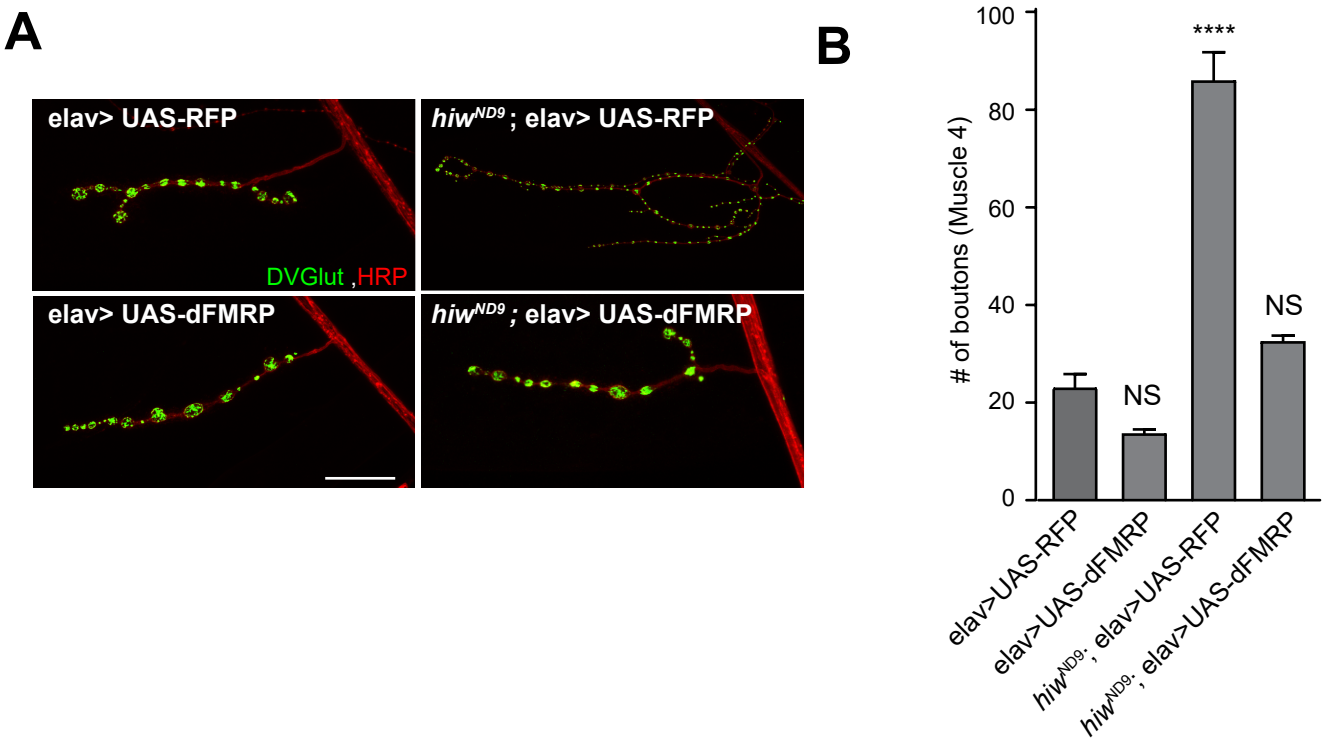

Figure S1, Related to Figure 1. Excess dFMRP does not alter NMJ growth in otherwise WT larvae, and suppresses overgrowth in a second *hiw* mutant background. (A) Representative images of the NMJ synaptic terminal at muscle 4 in third-instar larvae. For all genotypes, the pan-neuronal driver Elav-GAL4 was used to express the given transgene. NMJs were stained for the presynaptic bouton marker DVGLUT (green) and nerve membrane marker HRP (red). (B) Quantification of the mean (±SEM) number of DVGlut+ boutons per muscle 4 NMJ in each genotype, with each synaptic terminal contributing an n of 1. Overgrowth in this *hiw* allele was suppressed by dFMRP-overexpression, while dFMRP overexpression has no impact on basal NMJ growth. Statistical tests and exact p-values reported in Table S1. Scale bar = 25 µm. For all quantifications: * p= 0.05; ** p= 0.01; *** p = 0.001; **** p =0.0001, NS = not significant, p>0.05.

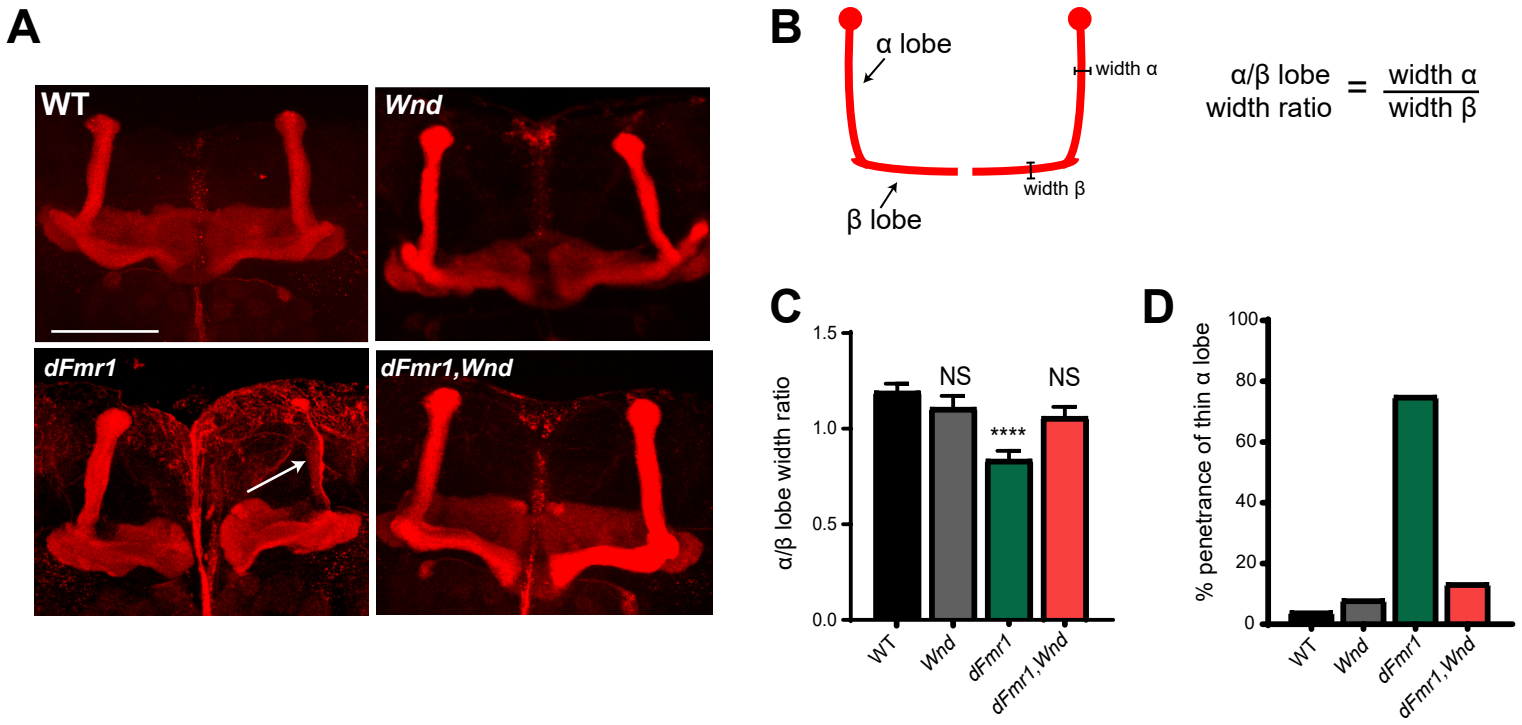

Figure S2, Related to Figure 3. Morphological abnormalities in *dFmr1* mushroom bodies are also Wnd-dependent. (A) Representative images of Drosophila mushroom bodies from WT, *Wnd* mutants, *dFmr1* mutants, and *Wnd,dFmr1* double mutants. Exact genotypes in **Table S1**. Antibody against Fasciclin II (FasII, Red) was used to label and visualize the α and β lobes of the mushroom bodies. The representative image for *dFmr1* illustrates a severe case of the thin α lobe phenotype (white arrow), which was the most prominent and common phenotype observed. (B) Schematic depicting α and β lobe projections and the measurements taken to define the α/β lobe width ratio for each mushroom body. (C) Quantification of the α/β lobe width ratio for all four genotypes. (D) Penetrance of the thin α lobe phenotype in each genotype. A thin α-lobe was defined as an α-lobe in which the absolute width (measured in microns) was two standard-deviations less than the mean α-lobe width for WT mushroom bodies. The total number of α-lobes that met this criterion were counted per genotype, and thus the penetrance of this phenotype is represented here. Scale bar = 50 μm.

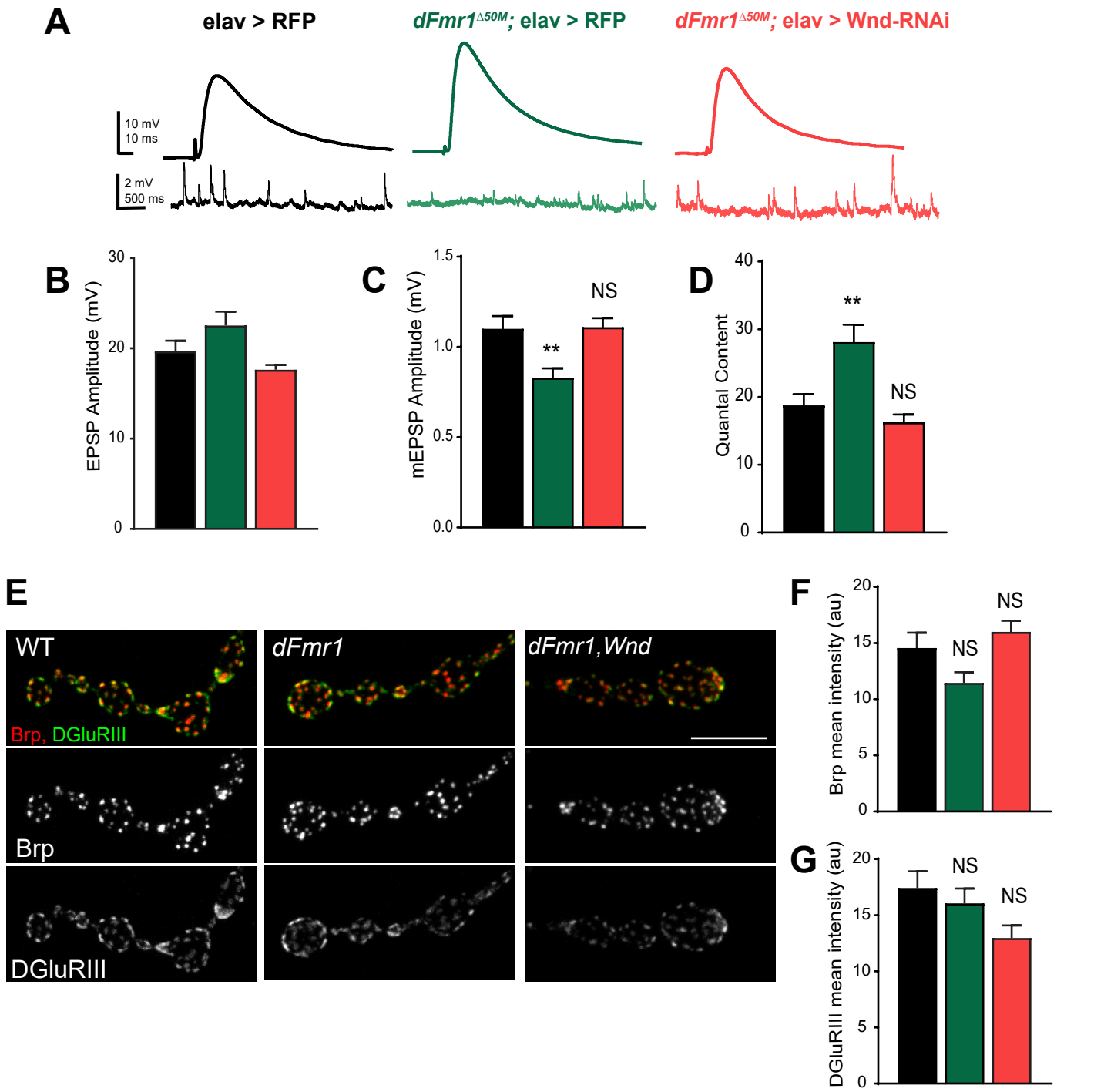

Figure S3, Related to Figure 4. Presynaptic Wnd drives abnormal synaptic transmission in *dFmr1* mutants, but active zone formation at *dFmr1* NMJs is grossly normal. (A) Representative EPSP and mEPSP electrophysiological traces from larval NMJs at Muscle 6. The pan-neuronal driver Elav was used to drive the control transgene UAS-RFP in either a WT background (elav > RFP), the *dFmr1* mutant background (*dFmr1*$^{\Delta 50M}$, elav>RFP), and we then knocked down Wnd by driving the Wnd-RNAi in the *dFmr1*$^{\Delta 50M}$, mutant background (*dFmr1*$^{\Delta 50M}$, elav>Wnd-RNAi). (B) Quantification of mean (±SEM) EPSP amplitudes, in which 75 consecutive evoked events were averaged per cell, and then cell amplitudes were averaged per genotype. (C) Quantification of mean (±SEM) mEPSP amplitudes, in which 75 consecutive spontaneous events were averaged per cell, and then cell amplitudes were averaged per genotype. (D) Quantification of quantal content, which was calculated individually per cell by dividing the mean EPSP amplitude by the mean mEPSP amplitude, and then averaged per genotype. This demonstrates that presynaptic Wnd is necessary for changes in synaptic transmission at the *dFmr1* mutant NMJ. (E) Representative images of WT, *dFmr1*, and *dFmr1,Wnd* NMJ boutons stained for the presynaptic scaffolding protein Brp (red) and the essential glutamate receptor subunits DGluRIII (also known as DGluRIIC - green). We did not observe differences in Brp or DGluRIII intensities in any genotype, nor were any apposition defects apparent, showing that synapse formation is largely intact in the absence of dFMRP. (F) Quantification of mean (±SEM) Brp intensity at the NMJ. (G) Quantification of mean (±SEM) DGluRIII intensity at the NMJ. Statistical tests and exact p-values reported in Table S1. For physiology, each cell recorded contributed an n of 1. For IHC, each NMJ terminal contributed an n of 1. Scale bar = 10 μm * p= 0.05; ** p= 0.01; *** p = 0.001; **** p =0.0001, NS = not significant, p>0.05.